

# Investigation of the Remolding Step in Reference Free

## Part Encapsulation

by

Paula J. Valdivia y Alvarado

Submitted to the Department of Mechanical Engineering  
in partial fulfillment of the requirements for the degree of

Master of Science in Mechanical Engineering

at the

MASSACHUSETTS INSTITUTE OF TECHNOLOGY

May 2000

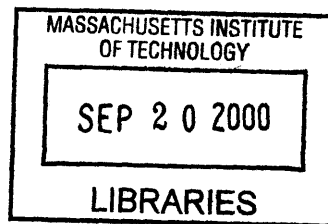
[June 2000]

© Massachusetts Institute of Technology, 2000. All Rights Reserved.

Author .....  
Department of Mechanical Engineering  
May 19, 2000

Certified by .....  
Sanjay E. Sarma  
Associate Professor of Mechanical Engineering  
Thesis Supervisor

Accepted by .....  
Ain A. Sonin  
Chairman  
Department Committee on Graduate Students



ARCHIVES



Room 14-0551  
77 Massachusetts Avenue  
Cambridge, MA 02139  
Ph: 617.253.2800  
Email: docs@mit.edu  
<http://libraries.mit.edu/docs>

## **DISCLAIMER**

**MISSING PAGE(S)**

56

# **Investigation of the Remolding Step in Reference Free Part Encapsulation**

by

Paula Valdivia y Alvarado

Submitted to the Department of Mechanical Engineering on May 19, 2000,  
in partial fulfillment of the requirements for the degree of Master of Science in Mechanical Engineering

## **Abstract**

As one of the most time and cost efficient methods to produce prototypes, machining also offers advantages such as precision and versatility. Fixturing is an essential consideration during machining as it presents several limitations to the machining capabilities, especially to cycle times and to the complexity of the geometry to be machined. In an attempt to overcome these limitations, extensive research developed flexible and universal fixturing systems.

Reference Free Part Encapsulation (RFPE) is one of such systems. It fixtures a workpiece by encapsulating it in a larger volume of a machinable Tin-Bismuth alloy. The process steps are a series of machining operations separated by remolding steps in the encapsulation machine, and by changes of setup. This work focused in the parameters that determine high quality remolding.

Several factors determine the quality of remolding during RFPE. The property selected to quantify the quality of remolding is the strength of the weldline between the existing encapsulant and the added one. The phase change during remolding and the resulting weldline were studied through a heat transfer model and also at a micro structural level.

The models were compared to the results of several tensile tests on remolded samples. Both the models and the experimental results determined a relation between solidification microstructure and quality of remolding. A set of temperatures for which the weldline is strong was established as well.

The determination of the optimal process temperatures will eliminate weak weldlines in remolded parts and at the same time will prevent accidental melting of the entire filler during remolding. This work will thus provide a process range for which RFPE will be most efficient.

Thesis Supervisor: Sanjay E. Sarma  
Title: Associate Professor of Mechanical Engineering

## Acknowledgments

My deepest gratitude goes to Professor Sanjay Sarma and Elmer Lee for their guidance and for letting me be a part of this project. Together with the members of RAMLab, they have made my graduate school experience one that I will look back at with fondness. Mark Belanger and Gerald Wentworth in the LMP machine shop were the most helpful, patient and enjoyable people to work with. To Professor Bora Mikic, thank you for the enlightening conversations on heat transfer, MIT and education.

My brother Pablo has been my family and confidant for five years. His friendship has given me much needed support and his dedication to pursuing his goals has given me inspiration. Nitza Basoco did the most wonderful thing for me, she showed me the meaning of true friendship. However, the strongest force behind my work is probably the one that is the furthest from MIT: my parents. They have taught me that no goal is too high and they have made me proud every single day of my life. I hope they realize that my achievements are theirs, as I am only a reflection of their love and upbringing.

To Miguel and Beli: los adoro y me hacen falta.

To the friends with whom I have grown and shared so many experiences in the undergraduate and graduate years at MIT: I have learned from you and the times we spent together more than I did in a semester of lectures.

I carry the knowledge, I carry the memories.

# Table of Contents

<b>Introduction .....</b>	<b>8</b>
1.1 Background on fixturing and the need for new techniques .....	8
1.2 Overview of methods that overcome fixturing limitations .....	9
1.3 Reference Free Part Encapsulation .....	11
1.4 RAMLab's Universal Fixturing System .....	13
1.5 RFPE challenges .....	16
1.5.1 Volume mismatch during remolding .....	17
1.5.2 Weldline strength .....	18
<b>Solidification .....</b>	<b>22</b>
2.1 Solidification microstructure .....	22
2.2 Eutectic solidification .....	24
2.3 Tin-Bismuth .....	27
<b>Solidification Model .....</b>	<b>29</b>
3.1 Heat Conduction model of the solidification problem .....	29
3.2 Determining the presence of phase change upon initial contact .....	29
3.3 Measuring the motion of the phase change interface .....	33
3.4 Solidification front velocity .....	38
3.5 Flow over the stock piece .....	38
<b>Experimental Determination of Weldline Strength .....</b>	<b>41</b>
4.1 Optimal weldline strength measurement .....	41
4.2 Sample preparation and test .....	42
4.3 Tensile test .....	45
4.4 Temperature relation .....	47
4.5 Observation of the cross sectional structure .....	49
<b>Interpretation of Results and their Application to Remolding in RFPE .....</b>	<b>51</b>
5.1 Relation between temperatures and weldline strength .....	51
5.2 Microstructure, growth rate and weldline strength .....	53
5.3 Conclusion .....	54
<b>References.....</b>	<b>57</b>

## List of Figures

Figure 1.1 Different Universal Workholding Techniques .....	10
Figure 1.2 Steps of the encapsulation process .....	12
Figure 1.3 Mini injector .....	13
Figure 1.4 Large injector .....	14
Figure 1.5 Illustration of the three fundamental machining strategies .....	15
Figure 1.6 Machining and encapsulation of orb samples- weldline broke in occasions.	19
Figure 1.7 Worst possible situations during remolding .....	21
Figure 2.1 Typical cast grain structure .....	24
Figure 2.2 Lateral diffusion during front advance .....	25
Figure 3.1 Determination of interface temperature on contact .....	30
Figure 3.2 Determination of heat transfer at the interface .....	31
Figure 3.3 Temperatures and their effect on phase change. ....	32
Figure 3.4 Motion of the solidification front .....	33
Figure 3.5 Motion of solidification front for different $T_m/T_l$ combinations ( $T_s=240$ )..	36
Figure 3.6 Motion of solidification front for different $T_m/T_l$ combinations ( $T_s=250$ )..	36
Figure 3.7 Motion of solidification front for different $T_m/T_l$ combinations ( $T_s=260$ )..	37
Figure 3.8 Motion of solidification front for different $T_m/T_l$ combinations ( $T_s=270$ )..	37
Figure 3.9 Front velocity for given solid and liquid temperatures .....	38
Figure 3.10 Heat transfer model including an embedded stock piece .....	39
Figure 4.1 Top half of mold.....	43
Figure 4.2 Bottom half of mold .....	43
Figure 4.3 Pouring of liquid alloy on a previously poured solid half-piece. ....	44
Figure 4.4 Comparative stress-strain plot of tested samples. ....	46
Figure 4.5 Representation of the order in which samples failed and temperatures at which they were prepared.....	47
Figure 4.6 Representation of the order in which samples failed and DT, the difference between temperatures at which they were prepared .....	48

Figure 4.7 Cross section of tensile test samples: from fastest failure to slowest.....	50
Figure 5.1 Time to failure vs. DT .....	52
Figure 5.2 Cross-section of a sample with fast fracture .....	53

## **List of Tables**

Table 1.1 Tin Bismuth properties (Eutectic composition: Sn 42% Bi 58%) .....	16
Table 1.2 Thermal properties of Bi-Sn in solid and liquid phases .....	16
Table 1.3 Mold Material Selection Data.....	18
Table 4.1 Combination of liquid and solid temperatures for each prepared sample .....	45



# Chapter 1

## Introduction

### 1.1 Background on fixturing and the need for new techniques

Despite the introduction of many new techniques, machining is still the most widely used process in the manufacturing of prototypes. It offers several advantages, such as precision, cost efficiency and quick delivery. However, it still presents some limitations, especially in the case of complex workpieces.

Fixturing is an essential element of a machining operation. Fixturing of a part refers to its immobilization, support and location. Locating the part is the initial fixturing step. In order to achieve the desired geometrical shape, it is necessary to position and locate the piece in space. Immobilization or holding is the next step. Clamping elements such as bolts, straps or clamps are applied in places that immobilize the piece as it is located, but also at the time when the machining forces become active. The supports need to be sufficient to absorb all the force loads applied to the workpiece.

Fixturing presents one of the biggest challenges for time efficient machining. A typical machining process requires bases, clamps, rest buttons, vises, parallels and sometimes modular fixtures as well as the expertise to select and design the appropriate fixturing assembly. This assembly depends on the complexity of the part to be machined and on the required toolpaths. It may require the construction of dedicated fixtures when the components are extremely intricate and such requirement increases machining time and cost. This practice presents additional shortcomings. For instance, the standard set of fixturing

devices limits the complexity of the shapes that can be machined [3], [20]. Indeed, fixturing is one of the most serious limitations to the versatility of machining.

The assembly of fixturing devices requires a skill that is not easily automated and is time consuming. It becomes particularly impractical for small batch or prototype production. This has presented a challenge for several applications, such as coated graphite components, which clearly shows the need to overcome these time limitations.

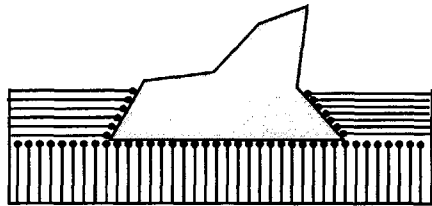
## **1.2 Overview of methods that overcome fixturing limitations**

Considerable research has been dedicated to overcome fixturing limitations and especially to reduce setup time. The design and improvement of modular and flexible fixtures increased the capabilities of a basic set of fixtures. Higher precision fixturing devices addressed accuracy and repeatability problems. More innovative fixturing techniques have also been developed. For instance, universal fixturing techniques are the focus of some recent research. These techniques allow machinists to fixture any part, independent of its geometry. Figure 1.1 illustrates the major categories among such techniques:

**Categories of Universal Work holding Techniques**

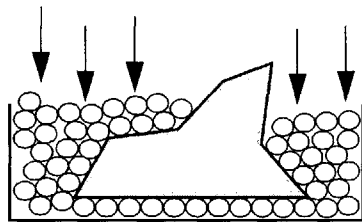
**Disadvantages**

**Bed of Fingers**



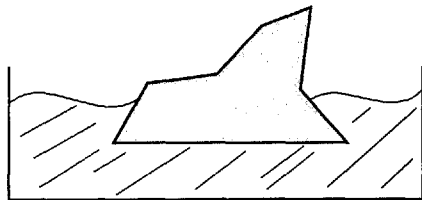
Fingers are unstable  
Provides little damping  
Interferes with toolpaths  
Mechanically complicated

**Fluidized Bed**



Instability due to voids  
Can not interfere with toolpaths  
Requires additional external forces

**Phase Change Encapsulation**



Hardware intensive  
Complex Process

Courtesy: Elmer Lee

**Figure 1.1** Different Universal Workholding Techniques

Among the universal fixturing techniques that have been suggested as solutions, phase change encapsulation methods are the most practical to implement and the most popular. The use of filler materials such as Cerro alloys and Rigidax polymer dates back to three

decades ago. The use of these low melting alloys or polymers is dedicated to immobilizing or shaping delicate and complex parts. However, despite the advantage it offers in setup time reduction and ease of fixturing, it has only been used in few applications at Pratt & Whitney Corporation and at Lawrence Berkeley Laboratories. Regular use of encapsulation is limited due to some practical constraints.

Encapsulation satisfies only two of the three purposes of fixturing. The three main purposes are location, support and immobilization. While encapsulation does a good job at immobilization and support, there are still some inconveniences with respect to location. The requirement of locating pins or die arrangements specific to the workpiece resembles the need for dedicated fixtures and the usual melt of the filler between setups loses all location information. These constraints, and the frequently high cost of low-melt alloys, result in a reduced use of encapsulation techniques.

### **1.3 Reference Free Part Encapsulation**

Fixturing usually requires a clamp or a vise and thus contact faces between the part and the fixturing device are not accessible for machining in a single setup. Several changes in setup are required in order to gain access to those faces and may cause a loss of location information. RFPE avoids this loss by virtually immobilizing the part in space. The virtual space around the stock piece is filled by the encapsulation, as shown in Figure 1.2. The resulting shape is easily fixtured and the exposed top surface can be machined. Once the machining operation is finished, the block is refilled with more molten filler and allowed to solidify. This is referred to as the remolding step.

Once this step is completed, a change of setup can take place. The original and new locations of the filler cube are exactly known, hence the location of the stock embedded inside is also exactly known. The machining and remolding steps described above can be

repeated until the features in the part are completed. In the final stage, the filler material is melted and recycled, freeing the completed component.

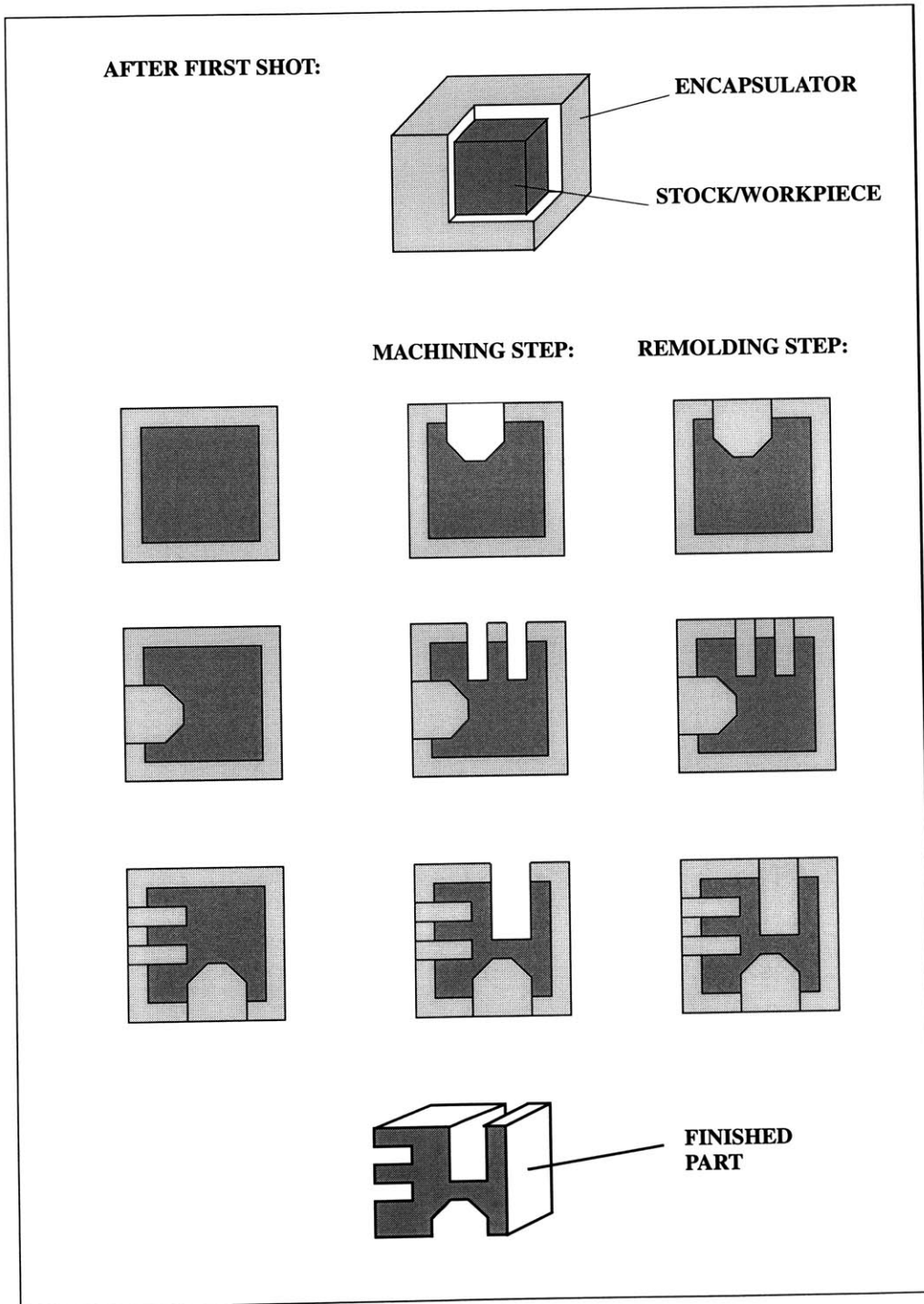


**Figure 1.2** Steps of the encapsulation process

### 1.4 RAMLab's Universal Fixturing System

The research conducted at MIT's Rapid Autonomous Machining Lab resulted in two versions of a system capable of implementing RFPE [12]. Both systems act on the same principle and their main difference is size. In addition to the mold in which the workpiece is held, the design includes a melter device, an injection system and a clamping system. The melter device or tank is a container which stores and heats the filler material. The injection system is a simpler version of injection molding machines used in industry: it injects the molten filler into the mold at a smaller shot size with lower pressure. The clamping system accepts different types of molds, insures their sealing and provides the necessary clamping against the injection pressure. Both the large scale system and the mini-injection system are shown in the figures below. The main components are indicated as well.

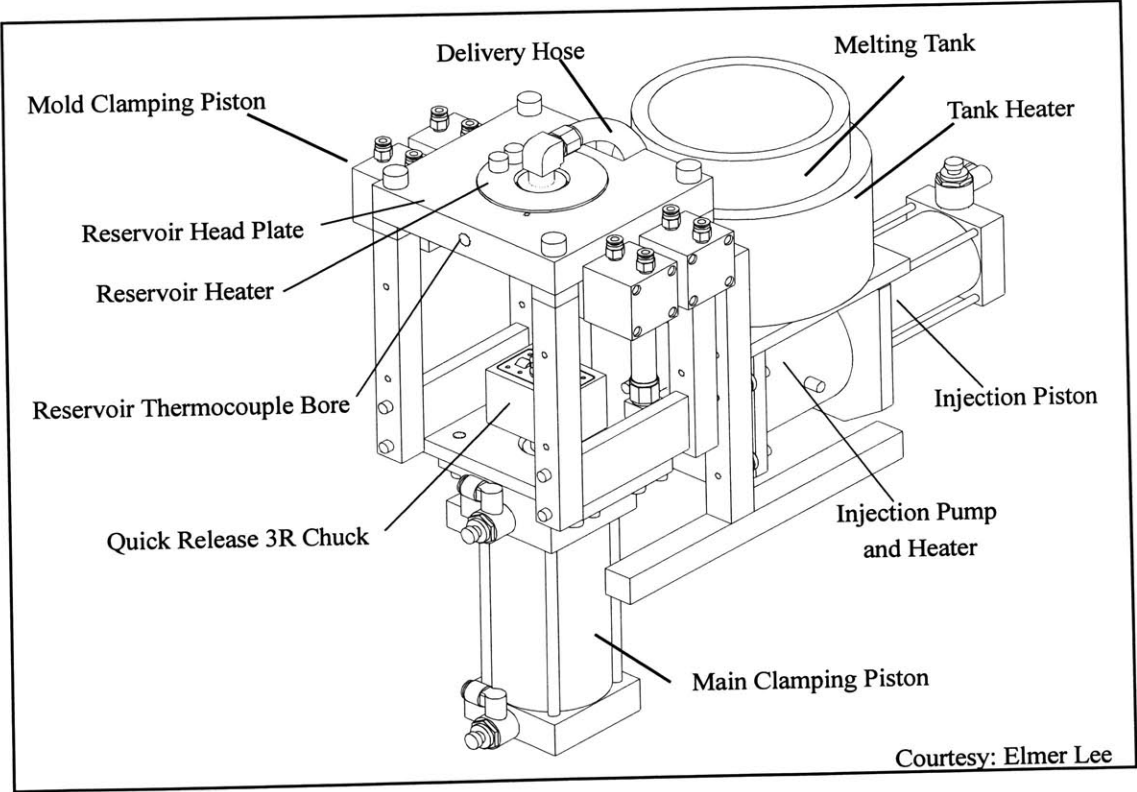
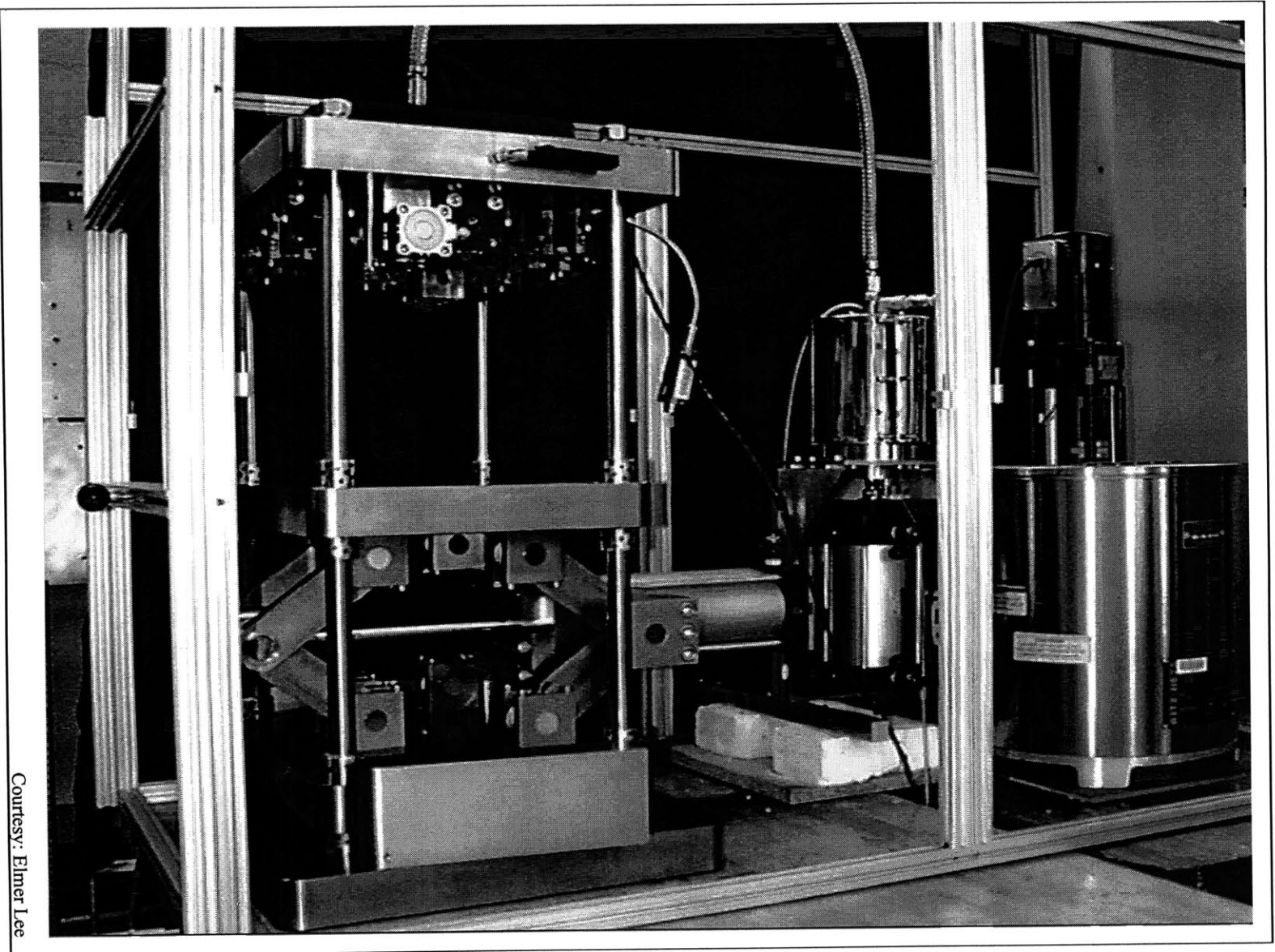


Figure 1.3 Mini injector



Courtesy: Elmer Lee

Figure 1.4 Large injector

Since machining requirements vary in size and complexity, different types of molds are needed to satisfy them. To accommodate most possible requirements, the universal systems uses three types of molds: 3-D milling, 2 1/2-D milling and 2-D milling molds. The parts encapsulated by these molds allow machining access to all its 6 sides, only 5 sides and only 2 opposite sides, respectively. Figure 1.5 illustrates the results of these molds and their corresponding machining strategies.

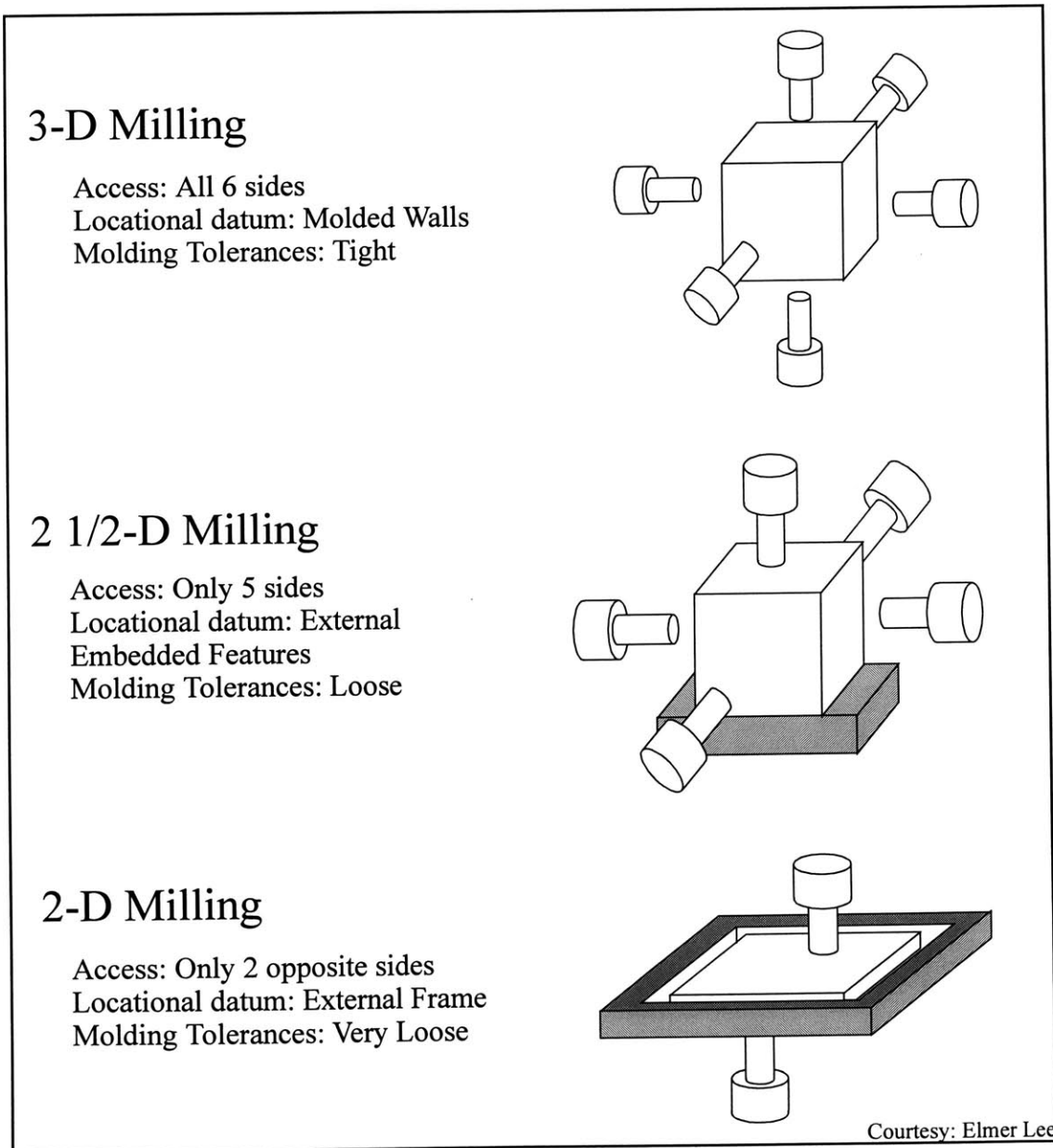


**Figure 1.5** Illustration of the three fundamental machining strategies



The encapsulator (filler material) used with this system is a eutectic composition of a Tin-Bismuth alloy. Other low melt materials are used in industrial phase-change fixturing. Machinable wax, such as Freeman™, and fixturing polymers such as Rigidax™ have been investigated as well. The choice of encapsulator was based on its strength, stiffness, machinability, thermal properties, quality of its adhesion to the workpiece, melting temperature, ease of reclaim, safety and cost. An overview of the alloy's properties [2] is provided in the tables below:

Property	Value
Tensile Strength, Ultimate (MPa)	69.4
Tensile Strength, Yield (MPa)	60.1 rising to 62.3
Modulus of Elasticity (MPa)	30,000.5
Hardness, Brinell	23
Melting Temperature (F); (K)	281; 411.48
Density (Kg/m <sup>3</sup> )	8,580
Latent Heat (J/Kg)	44798.70485

**Table 1.1 Tin Bismuth properties (Eutectic composition: Sn 42% Bi 58%)**

Thermal Property	Solid Phase	Liquid Phase
Thermal Conduction Coefficient k (W/m.K)	18.5	18.5
Coefficient of Thermal Expansion (μm/m-°C)	20.8	
Specific Heat c	167	155
Thermal Diffusivity $\alpha = k/cp$	1.2911e-005	1.3911e-005

**Table 1.2 Thermal properties of Bi-Sn in solid and liquid phases**

### 1.5 RFPE challenges

Testing of the RFPE system described above was performed mainly in the small (2 1/2-D) machine. The results are overall satisfactory, but there are still some challenges to overcome.

### **1.5.1 Volume mismatch during remolding**

At the beginning of the encapsulation process, the stock material is placed inside the mold. The mold is closed, clamped in the system and filled with the liquid alloy. This is the first shot. After the first shot, the part is taken to be machined and then brought back to the encapsulation system for the remolding step. An initial challenge to remolding was the volume mismatch between the mold cavities and the cooled part. Immediately after injection, the filler alloy solidified while the mold was still at a high temperature and thus under thermal expansion. After the part was removed, the mold cooled and returned to its original volume. The difference between the mold's and the filler's coefficients of thermal expansion is responsible for their volume mismatch.

The problem presented by this mismatch can be solved in two ways. One is to select a mold material with a similar coefficient of thermal expansion to that of the filler alloy. The second option is to maintain the mold at a high enough temperature such that it will have expanded and will fit the part during all remolding steps. The latter is a more demanding procedure because it requires continuous additional heating sources around the mold. It is also more cumbersome to determine the exact temperature at which the mold must be kept and there is an added risk of losing location information in case the mold cavity expands to a dimension larger than that of the part.

The first option is best suited to solve the mismatch problem. The mold material must be chosen such that its CTE is closer to that of the alloy assuming that the mold and encapsulation are kept at the same temperature during process. The materials studied for this purpose are listed below. The selection takes into consideration the material's coefficient of thermal expansion, machinability, thermal conductivity and cost. Metals such as steel satisfy the CTE and machinability requirements. Their thermal expansion is low and they are often easy to machine. However, metals are also good heat conductors. This is an

undesirable quality for the mold material because if the mold heats up too fast, the cooling time becomes too long and so does the entire cycle time. Ceramics and composites also have a low coefficient of thermal expansion, often lower than that of metals. Their thermal conductivity is low, making them good insulators and thus an appropriate choice for cycle time reduction [15]. The shortcoming of several of these materials is their machinability. Ceramics are very brittle and composites such as those used for the electronics industry are manufactured in small dimensions, at high production costs. However, some machinable ceramics are available. The selected material, Mica 1100, is a machinable ceramic that can be machined in the same way as steel.

	Aluminum	Invar 36	Steel	Graphite	Aluminum Nitride	Silicon Carbide	Tin-Bismuth	Ultem	Mica 1100	Macor	Alumina Silicate
Density (g/cc)	2.72	8.05	7.858	2.25	3.25	3.21	8.58	1.27	2.768	2.52	3.96
Brinell Hardness	90		163				23		56		
Ultimate Tensile Strength (MPa)	360	621	555				69.4	105			310
Yield Tensile Strength (MPa)	205	483	350				56.2	104.8	34.47		
Modulus of Elasticity (GPa)	69	148	200	4.8		430	30.5		73.08		366
CTE, linear ( $\mu\text{m}/\text{m}\cdot^\circ\text{C}$ )	23.2	1.3	11.5	2	4.3		20.8	55.8	16.92		7.4
Thermal Conductivity (W/m-K)	160	10.15	51.9	24	155	110	18.5		0.586	1.44	19
Melting Point C	565	1427		3650						1250	1745

**Table 1.3 Mold Material Selection Data**

### 1.5.2 Weldline strength

During remolding, the liquid alloy injected into the mold is in contact with the machined surfaces of the workpiece and the solid encapsulant. The adhesion of the newly

injected liquid alloy to the workpiece is similar to that during the initial shot. Its adhesion to the solid encapsulant is referred to as the weldline.

The weldline strength is important because it determines how well the fixturing system withstands machining forces. This strength is not easily quantifiable, as the volumes of encapsulant to be injected vary each time. However, regular use of the system showed that although remolding completely filled the workpiece and its encapsulation, the weldline was not strong enough.

The weakness of the weldline was detected during the machining of an orb sample. This shape is formed by the intersection of two cylinders. The machining process is a sequence of drilling and milling operations, with setup changes in between (a 90 degrees rotation of a 2 1/2-D sample). During the second visit to the machine center (after initial shot and first remolding), the part broke off at the weldline.

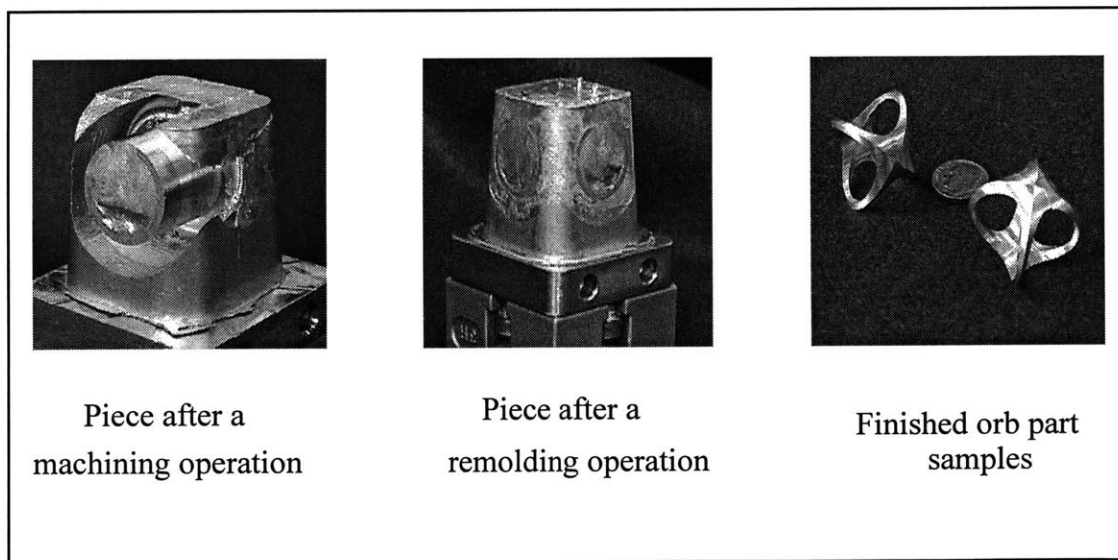


**Figure 1.6** Machining and encapsulation of orb samples- weldline broke in occasions

The weldline weakness was originally interpreted as contamination by the coolant and debris of the machined material. However, the weldline remained weak even for those samples that were carefully cleaned between machining and remolding.

This weakness is rather caused by a lack of good cohesion between the solidified liquid alloy that is injected during remolding and the alloy that is already. The mold temperature was well below the alloy's melting temperature and maintained the solid alloy it contained in a solid phase. The liquid alloy injected in this cavity did not have a high enough temperature to melt the alloy and thus they could not fuse to form a unified blend.

On the other hand, if the liquid alloy being injected was at a much higher temperature, there was a risk of melting all the alloy already present in the cavity. This would guarantee a uniform blend of alloy around the part and also a strong holding force provided by the alloy. However, this would allow the workpiece to shift position within the encapsulant and cause the loss of location information for the part.

These two extreme cases show the necessity of determining with precision an adequate range of operating temperatures for the remolding step. These temperatures need to be such that the liquid alloy injected into the cavity melts a layer of the solid alloy already present and not its entirety. This would assure a strong weldline without the risk of melting all the alloy and consequently losing the part's location information.

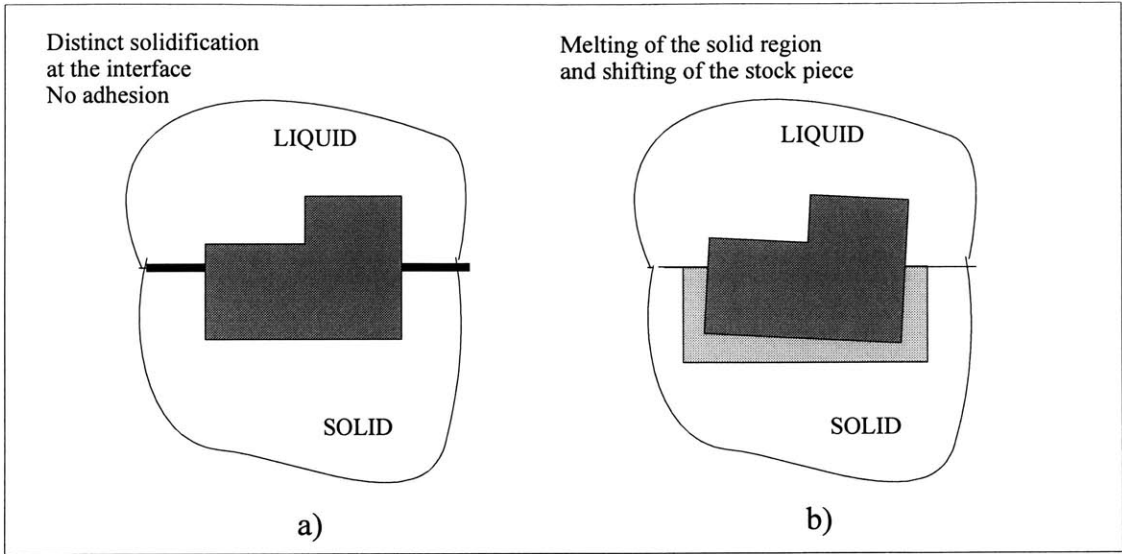


**Figure 1.7** Worst possible situations during remolding

# Chapter 2

## Solidification

The properties of alloys are strongly dependent on their microstructure, which describes the grain structure and the combination of phases present in a material, as well as its defects, morphology and distribution. Generally, for a material of a given composition, the microstructure is not constant and varies greatly, depending on processing conditions [13]. This chapter studies the formation of the microstructure in the encapsulation alloy in order to determine its solidification conditions and to better understand the solidification mechanism and the structure it leads to.

During solidification, solute redistribution at the interface and the diffusion in the liquid and in the solid lead to the final segregation profile. This profile may range from a high solute concentration in the region that solidified last to a uniform distribution. This region may be as small as a dendrite arm ( $l$  between 10 and 100mm) or as large as a macroscopic bar ( $l$  around 100mm). A dendrite arm typically thickens at a very slow rate and thus the boundary layer  $d$  is much greater than  $l$ . This means that diffusion will maintain a uniform  $C_L$  throughout the liquid during solidification.

Diffusion in the solid is sometimes so fast that the composition is maintained uniform in the case of interstitial solutes. For substitutional solutes, diffusion is much slower and can usually be neglected.

### 2.1 Solidification microstructure

The solute redistributed at the interface is commonly rejected into the liquid and accumulates into a solute boundary layer. This accumulation can cause the front to form cells

or dendrites. The liquid ahead of the front may be constitutionally undercooled (below its melting temperature yet at a temperature higher than the liquid at the front). In this case, the plane front becomes unstable since a bump on the interface penetrates into undercooled liquid, where it grows more quickly.

A maximum velocity to avoid constitutional undercooling is:  $V_{max} = -\frac{D_L G k}{m_L C_o (1 - k)}$ , where  $m_L$  is the gradient of the liquidus line on the phase diagram (usually negative). This critical velocity is very low, so it is usually very difficult to avoid constitutional undercooling unless in the case of highly pure materials.

When constitutional undercooling occurs, the planar growth becomes unstable and can break into cells and dendrites. If the undercooling is relatively weak, the interface breaks into a semi-sinusoidal form and generates cells. If the undercooling is strong (for a velocity higher than  $V_{max}$ ), side branches form and develop into a dendritic structure.

In the case of castings, solidification generally occurs with a dendritic structure. The given direction of the dendrite growth affects the general grain structure of the casting. When liquid metal is poured into the mold, the initial contact with the cold walls usually results in nucleation of many crystallites and forms the chill zone. Solidification occurs from each of these crystallites, with the dendrites oriented in the direction parallel to the heat flow direction (faster growth). Crystals in other directions grow at a slower pace and tend to get squeezed by their neighbors.

The fast growing crystals form columnar shapes which in their turn conform the columnar zone. This zone may extend to the central plane of the casting. However, often fragments detach from the dendrites and remain ahead of the columnar grains. These randomly oriented crystals are reunited at the center of the mold and form a central equiaxed zone.



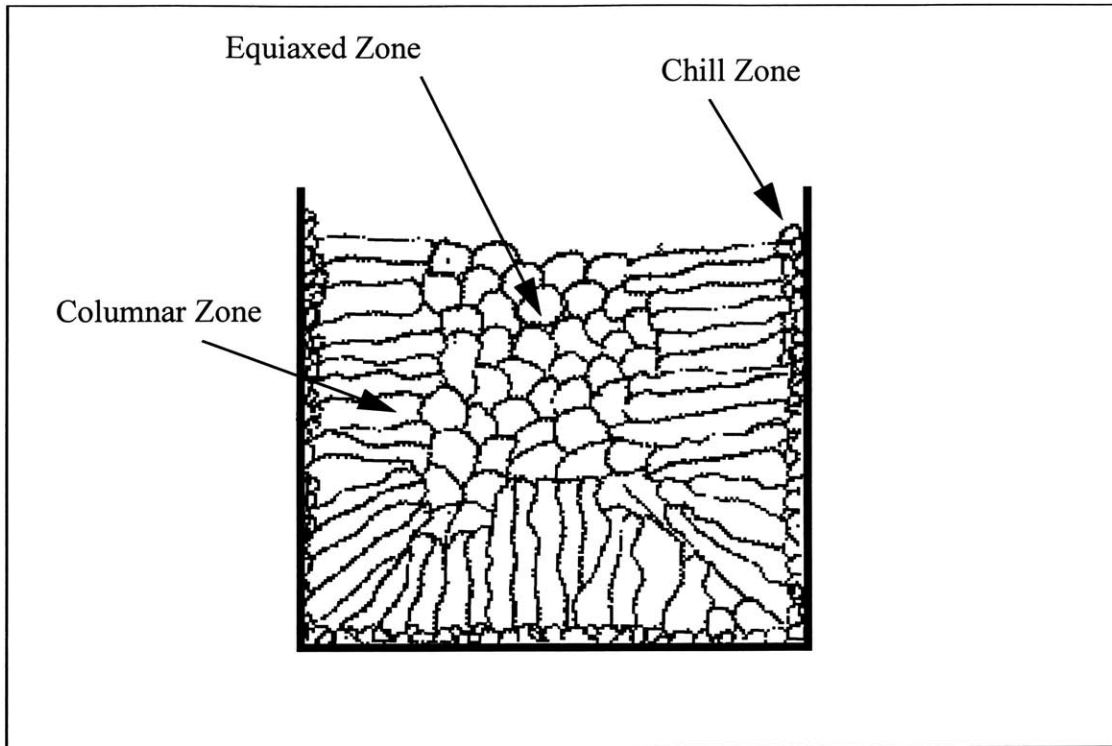


**Figure 2.1** Typical cast grain structure

## 2.2 Eutectic solidification

For a typical eutectic system of components A and B and a given undercooling on the growth front, a minimum lamellar spacing can be predicted. A space larger than this minimum facilitates the advance of the growth front.

Eutectic alloys are attractive for casting applications for their good fluidity, little tendency to form pores and exhibit hot tearing. This is mainly because they lack a mushy zone during solidification. The phase diagram and corresponding free energy curves are the best way to determine the growth mode of the solidification front.

During solidification, the temperature falls below  $T_{Am}$  and there is a (decrease in energy) driving force for liquid of composition  $C_{Col}$  to transform into a mixture of  $\alpha$  and  $\beta$  phases [6]. These two phases grow behind the solidification front. While the A-rich  $\alpha$  phase solidifies, excess B is diffused laterally and is incorporated in the B-rich  $\beta$  phase.

Similarly, excess A is diffused from the  $\beta$  phase into the  $\alpha$  phase. The speed of this diffusion determines the growth of the solidification front. This in turn depends on the inter-lamellar spacing  $\lambda$ . The smaller the spacing, the faster the front grows.

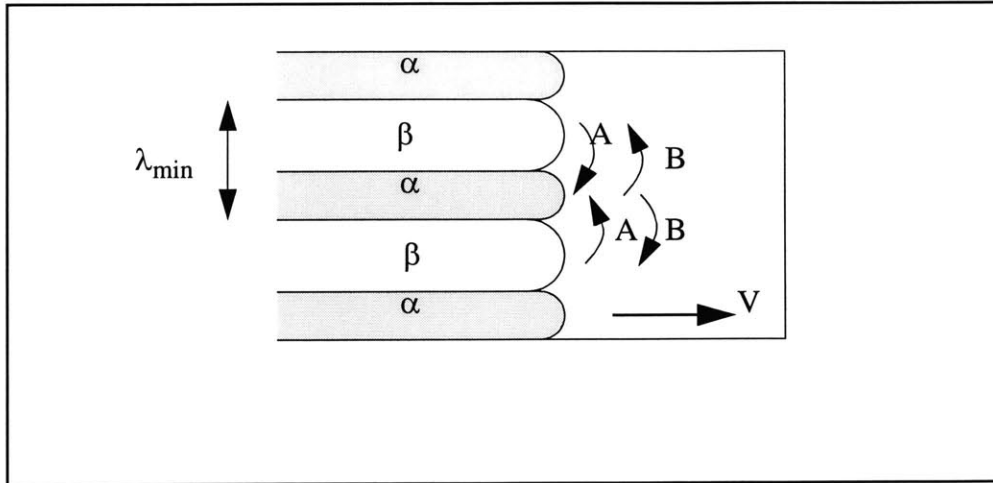


**Figure 2.2** Lateral diffusion during front advance

These usually form as lamellae of  $\alpha$  and  $\beta$  with orientation parallel to the growth direction. Sometimes they form as rods of B in an  $\alpha$  matrix if the proportion of B is low. While the mix shape assumes a lamellar eutectic morphology, there is an energy change in the  $\alpha/\beta$  interface. The  $\alpha/\beta$  interfacial area created per  $m^3$  is  $(2/\lambda) m^2$ , where  $\lambda$  is the lamellar spacing. Therefore, for an interfacial undercooling of  $\Delta T_0 = T_e - T_*$ , the net free energy charge is:

$$\Delta G = \frac{\Delta H_f \Delta T_0}{T_e} + \frac{2\gamma_{\alpha\beta}}{\lambda}$$

where  $\gamma_{\alpha\beta}$  is the interfacial energy in  $J.m^{-2}$ . This can be accounted for in the free energy plot by raising the  $\alpha$  and  $\beta$  curves to account for the energy associated with the interface. For a given undercooling  $T_0$ , setting the change in energy to zero will result in

the minimum lamellar spacing  $\lambda_{min} = \frac{2\gamma_{\alpha\beta}T_e}{\Delta H_f\Delta T_0}$  (where the kinetic undercooling was assumed to be negligible)

Besides adsorption onto the solid and formation of the  $\alpha/\beta$  interface, there is also redistribution of solute by diffusion in the liquid next to the solidification front. The driving force for diffusion comes from the total free energy. Part of the undercooling is used to generate the  $\alpha/\beta$  interface (for a  $\lambda$  greater than  $\lambda_{min}$ ), the rest of the undercooling drives the solute lateral diffusion.

The undercooling generates the free energy that drives the a/b interface and that also drives the lateral diffusion of solute. The location of the 3 free energy curves is determined by fixing  $\lambda$  and the undercooling  $\Delta T_0$ . The concentrations of the liquid in equilibrium with phases  $\alpha$  and  $\beta$  are thus defined. If we assume these concentrations to remain constant, the difference  $\Delta C$  between them and  $\lambda$  determine the concentration gradient for lateral diffusion. The relation is:

$\Delta C \approx \Delta C_0 \left(1 - \frac{\lambda_{min}}{\lambda}\right)$  where  $\Delta C_0$  is the concentration difference when  $\lambda$  tends to infinity. For a fixed undercooling, an increase in  $\lambda$  from  $\lambda_{min}$  initially increases and then decreases the concentration gradients.

The advance velocity of the solidification front depends on the rate of solute partitioning in the liquid and thus to the lateral flux of solute ( $= D \frac{\partial C}{\partial y}$ ). The front velocity can then be expressed as:

$$V = B_1 D_L \left(\frac{\Delta C}{\lambda}\right)$$

where  $B_1$  is a constant and  $D_L$  is taken as the interdiffusion coefficient for both solutes. Inserting the relation above into this expression, we obtain:

$$V = B_2 D_L \Delta T_0 \left(\frac{1}{\lambda} - \frac{\lambda_{min}}{\lambda^2}\right) \quad \text{(It was also noted that } \Delta C_0 \text{ is proportional to } \Delta T_0\text{).}$$

$B_2$  is another constant which in practice has a typical value around  $0.1\text{K}^{-1}$ . Since  $\lambda_{\min}$  is known, the solidification front velocity can be determined as a function of the inter-lamellar spacing. There will be a particular spacing that will result in the maximum solidification velocity. This spacing is found by equating the derivative of  $V$  with respect to  $\lambda$  to zero.

$$\frac{dV}{d\lambda} = B_2 D_L \Delta T_0 \left( -\frac{1}{\lambda^2} + \frac{2\lambda_{\min}}{\lambda^3} \right) = 0 \quad .$$

The maximum velocity is obtained under extremum conditions, which are common for most eutectic systems. The extremum spacing resulting in such velocity is  $\lambda_e = 2\lambda_{\min}$  .

Introducing the extremum spacing in the expression for the solidification velocity results in:  $V = \frac{B_2 D_L \Delta T_0}{4\lambda_{\min}}$

$$V = \frac{B_2 D_L \gamma_{\alpha\beta} T_e}{2\lambda_{\min}^2 \Delta H_f}$$

$$V\lambda^2 = \frac{B_2 D_L \gamma_{\alpha\beta} T_e}{\Delta H_f}$$

The right hand side of the equation is constant for a given eutectic system and has a typical value of  $10^{-16} \text{ m}^3\text{s}^{-1}$ . Finer lamellar spacings are thus associated with faster growth.

A small fraction of eutectic systems don't grow at extremum conditions. They show a wider range of lamellar spacings and in average this spacing is much larger than that of extremum growth. These spacings are irregular and vary between a lower limit of the extremum lamellar case and an upper limit  $\lambda_b$  at which the faceted phase branches. These are known as anomalous eutectics.

### 2.3 Tin-Bismuth

At moderate cooling rates, the eutectic Sn-Bi microstructure is lamellar, with degenerate material at the boundaries of the eutectic grains. This microstructure is similar to the one theoretically predicted for relatively slow cooling rates. Researchers observed cracks

on slowly cooled eutectic Sn-Bi joints. Slow cooling results in the formation of large grains. Tin precipitated from the solder matrix along the boundaries of the large grains through which cracking occurred. Cracking was not observed during rapid cooling. Cooling rates, however, were not specified in literature.

Thus the quality of the solidification microstructure depends on the cooling rate. The application of high cooling rates or high undercoolings can establish a rapid solidification process in metallic alloys [4]. They can be applied with the reduction or elimination of nucleation sites. This results in appealing microstructures, such as fine grains and homogeneous structures without solute segregation.

## Chapter 3

### Solidification Model

Different methods help determine the velocity of the solidification front during remolding. At the molecular level, the solid front growth velocity is determined by the solidification structure. In the macro scale, the solidification of the refill alloy can be modeled as a purely heat conduction problem.

#### **3.1 Heat Conduction model of the solidification problem**

The solidification of the alloy injected during remolding can be represented by a heat conduction problem. The model first accounts for the initial contact of the solid and liquid bodies which are at different temperatures, determines the interfacial temperature and the presence of phase change. Then, the model accounts for the advance of the phase change front.

#### **3.2 Determining the presence of phase change upon initial contact**

The first way to determine whether bringing a hot liquid in contact with a cooler solid will cause melting of the latter or solidification of the former is to determine the interface temperature at contact and its relation to the alloy's melting temperature [1].

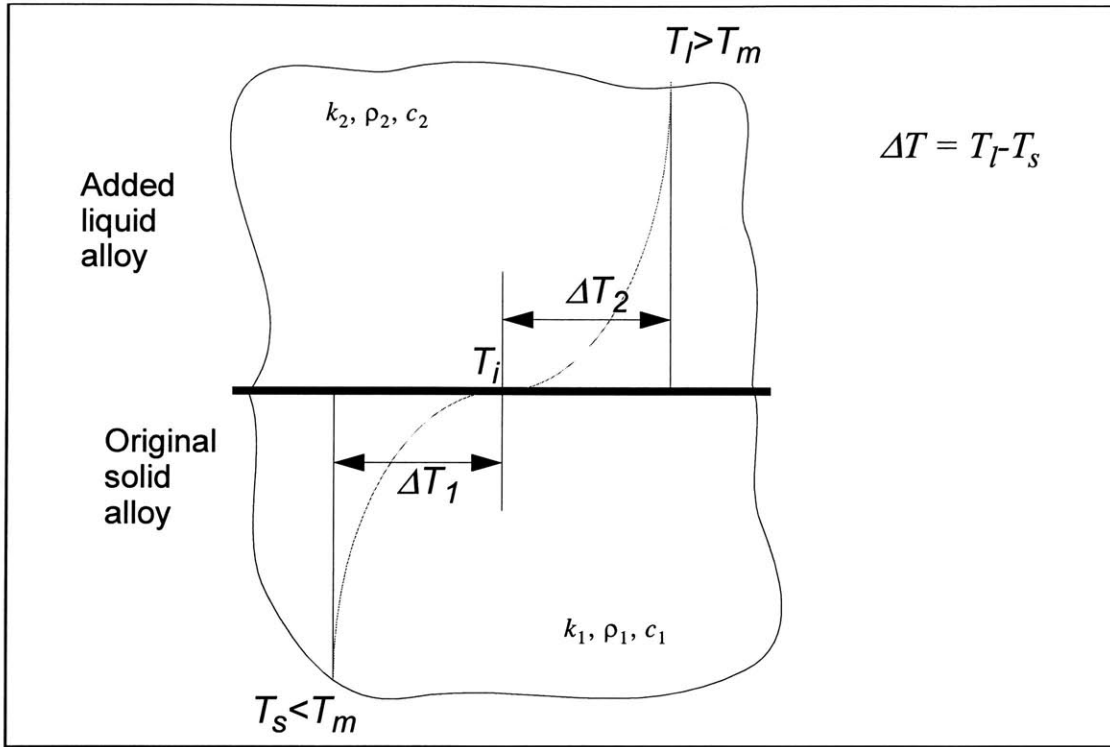


**Figure 3.1** Determination of interface temperature on contact

It is possible to find the interface temperature  $T_i$  at contact. If this temperature is greater than the alloy melting temperature  $T_m$ , the solid will melt. On the other hand, if  $T_i$  is smaller than  $T_m$ , the liquid will solidify. We find  $T_i$  by heat flux equilibrium at the interface.

$$q''_1 = q''_2$$

$$k_1 \frac{\Delta T_1}{\sqrt{\pi \alpha_1 t}} = k_2 \frac{\Delta T_2}{\sqrt{\pi \alpha_2 t}}$$

$$\frac{\Delta T_1}{\Delta T_2} = \frac{\sqrt{(k\rho c)_2}}{\sqrt{(k\rho c)_1}} \text{ or}$$

$$\frac{T_i - T_s}{T_l - T_i} = \frac{\sqrt{(k\rho c)_2}}{\sqrt{(k\rho c)_1}} \text{ which simplifies to}$$

$$T_i = \frac{T_l \sqrt{(k\rho c)_2} + T_s \sqrt{(k\rho c)_1}}{\sqrt{(k\rho c)_1} + \sqrt{(k\rho c)_2}}$$

This expression [12] allows thus to determine whether the  $T_l$  and  $T_s$  temperatures used during remolding will result in melting or solidification. Melting is desired, since solidification will later occur due to cooling and heat removal by the mold walls. However, initial melting ensures a better bond of the solidified liquid to the previous solid.

A second and similar method to determine if the phase change is solidification or melting is by assuming the interface temperature to be initially at  $T_m$ . The heat flux into the solid and out of the liquid can then be determined. If they are different, there is no equilibrium and thus there is phase change. The sign of the heat flux difference determines whether there is melting or solidification:

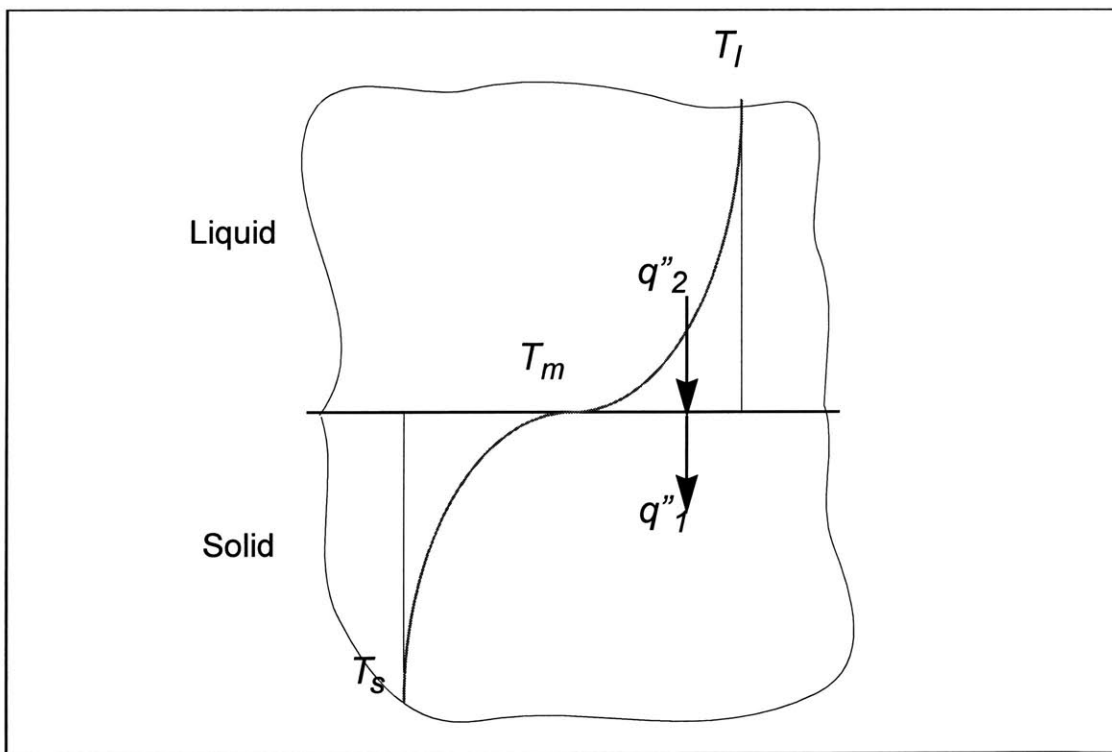


**Figure 3.2** Determination of heat transfer at the interface

From the temperature profiles for transient conduction in a semi-infinite body, the heat transfers are determined to be



$$q''_1 = \frac{k_1(T_m - T_s)}{\sqrt{\pi\alpha_1 t}} \text{ and } q''_2 = \frac{k_2(T_l - T_m)}{\sqrt{\pi\alpha_2 t}}$$

If the  $q''_1 - q''_2 \neq 0$ , then there is phase change. These two methods are equivalent and they result in a relation of  $T_m$  to  $T_l$  for which phase change will start. This relation is illustrated below.

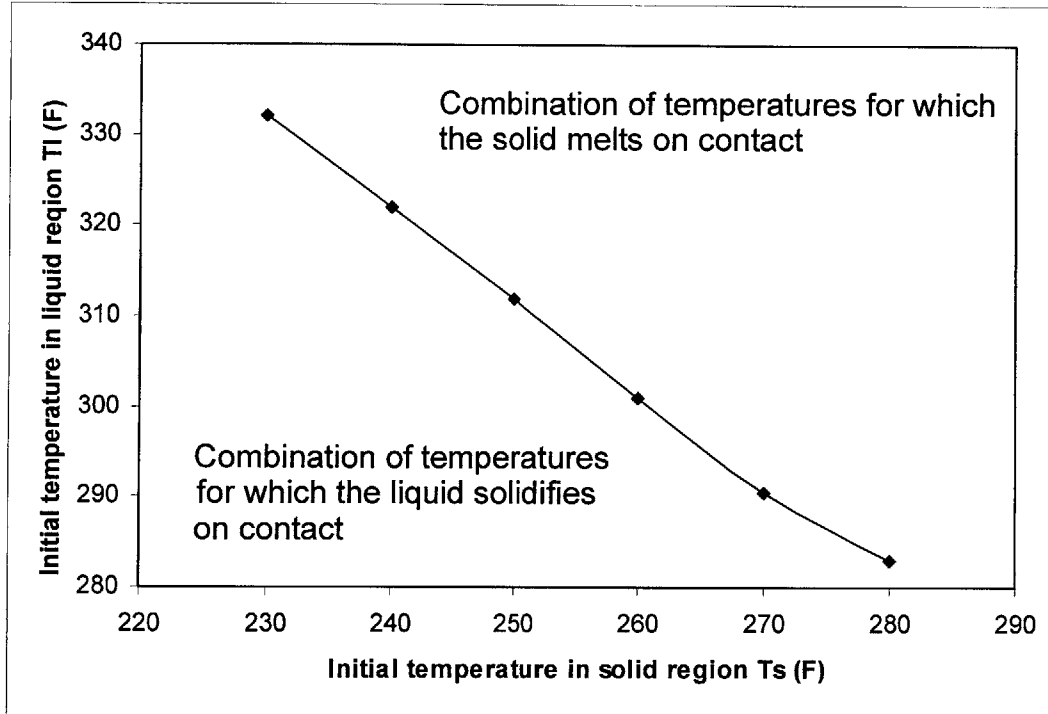


**Figure 3.3** Temperatures and their effect on phase change.

Once the type of phase change is determined, it is also possible to determine the penetration depth of the initial melting. Melting was determined by the inequality of the heat fluxes in the solid and liquid regions. This meant that in order to satisfy heat balance, phase change was required. In a comparison of heat fluxes, the difference  $q''_1 - q''_2$  is equal to the heat corresponding to phase change. This is the latent heat term, given by  $\rho L \frac{dX}{dt}$ , where  $L$  is the latent heat of the material and  $X$  is the length of the solidified material.

Samples prepared at temperatures to the right of the line in Figure 3.3 are expected to have a stronger weldline.

### 3.3 Measuring the motion of the phase change interface

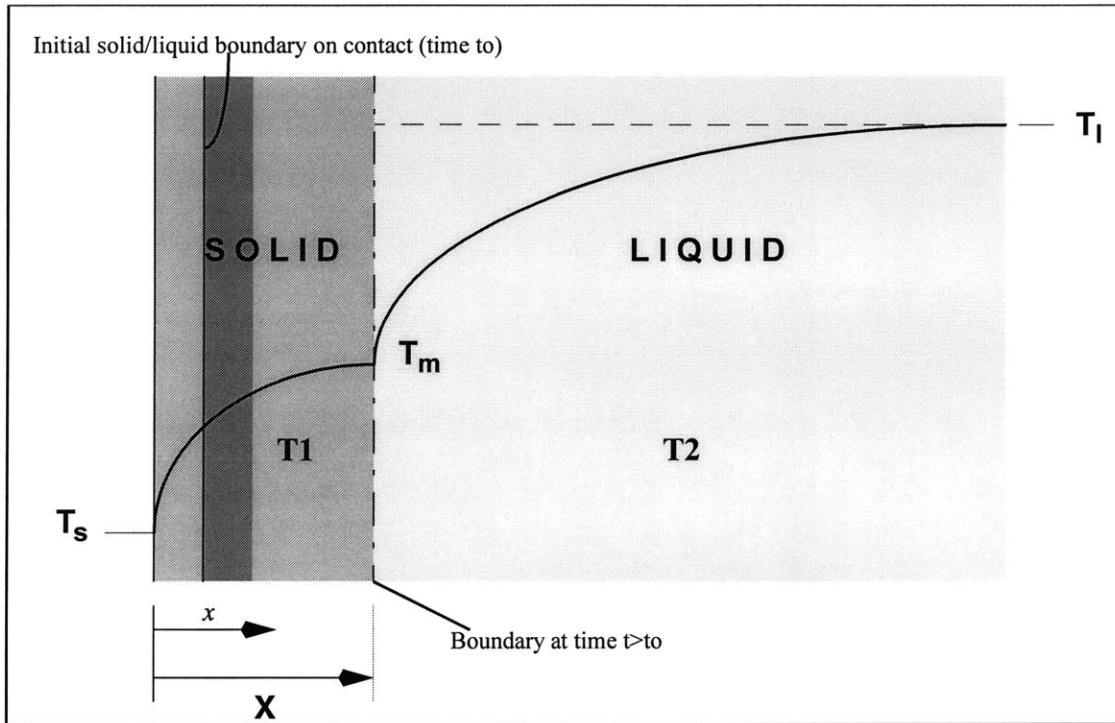


**Figure 3.4** Motion of the solidification front

The system is studied using a semi-infinite body heat transfer model [5], [8]. The temperature and properties corresponding to the solid and liquid regions are indexed 1 and 2, respectively.

The governing equation for temperature in each region is the Fourier equation:

$$\frac{\partial T_1}{\partial t} = \alpha_1 \frac{\partial^2 T_1}{\partial x^2} \quad \text{and} \quad \frac{\partial T_2}{\partial t} = \alpha_2 \frac{\partial^2 T_2}{\partial x^2}$$

where  $\alpha$  is the diffusivity term. The boundary conditions in the liquid region are

$$T_2 = T_l \text{ at } x \rightarrow \infty \text{ and in the solid region } T_1 = T_s \text{ at } x = 0 .$$

$$\text{At } x = X, T_1 = T_2 = T_m .$$

The depth of solidified liquid is  $X = b\sqrt{t}$ , where  $t$  is time and  $b$  is a constant.

The non-dimensionalized temperatures and corresponding Fourier equations are:

$$\theta_1 = T_1 - T_m,$$

$$\theta_2 = T_2 - T_m,$$

$$\theta_s = T_s - T_m,$$

$$\theta_l = T_l - T_m,$$

$$\frac{\partial \theta_l}{\partial t} = \alpha \frac{\partial^2 \theta_l}{\partial x^2} \text{ and } \frac{\partial \theta_l}{\partial t} = \alpha \frac{\partial^2 \theta_l}{\partial x^2} \text{ with boundary conditions:}$$

$$\theta_1 = \theta_s \text{ at } x = 0,$$

$$\theta_1 = 0 \text{ at } x = X,$$

$$\theta_2 = 0 \text{ at } x = X,$$

$$\theta_2 = \theta_l \text{ when } x \rightarrow \infty$$

The solutions are:

$$\theta_1 = \theta_s \left( 1 - \frac{\operatorname{erf}\left(\frac{x}{\sqrt{4\alpha_1 t}}\right)}{\operatorname{erf}\left(\frac{b}{\sqrt{4\alpha_1}}\right)} \right) \text{ and } \theta_2 = \frac{\theta_l}{\operatorname{erfc}\left(\frac{b}{\sqrt{4\alpha_2}}\right)} \left( \operatorname{erf}\left(\frac{x}{\sqrt{4\alpha_2 t}}\right) - \operatorname{erf}\left(\frac{b}{\sqrt{4\alpha_2}}\right) \right)$$

The non homogeneous boundary conditions at the solidification front is the energy equilibrium equation:

$$q_1'' - q_2'' = \rho L \frac{dX}{dt}$$

The heat flux in each case is:

$$q_1'' = -k_1 \left( \frac{\partial T_1}{\partial x} \right) \Big|_{x=b\sqrt{t}} = -\theta_s \sqrt{(k\rho c)_1} \frac{\exp\left(\frac{-b^2}{4\alpha_1}\right)}{\operatorname{erf}\left(\frac{b}{\sqrt{4\alpha_1}}\right)} \frac{1}{\sqrt{\pi t}}$$

$$q_2'' = -k_2 \left( \frac{\partial T_2}{\partial x} \right) \Big|_{x=b\sqrt{t}} = -\theta_s \sqrt{(k\rho c)_2} \frac{\exp\left(\frac{-b^2}{4\alpha_2}\right)}{\operatorname{erfc}\left(\frac{b}{\sqrt{4\alpha_2}}\right)} \frac{1}{\sqrt{\pi t}}$$

Inserting these expressions in the energy equation above and introducing new nondimensionalization terms results in:

$$\frac{\exp(-\delta^2)}{\operatorname{erf}(\delta)} + \theta\beta \frac{\exp\left(-\delta^2 \frac{\alpha_1}{\alpha_2}\right)}{\operatorname{erfc}\left(\delta \sqrt{\frac{\alpha_1}{\alpha_2}}\right)} = \sqrt{\pi} \delta S_n$$

where

$\delta = \frac{b}{\sqrt{4\alpha_1 t}}$  is the nondimensional term that represents time and displacement for the solidification front,

$\theta = \frac{T_l - T_m}{T_m - T_s}$  is the ratio of temperature differences.

$\beta = \sqrt{\frac{(k\rho c)_2}{(k\rho c)_1}}$  is a term grouping the material properties.

In this expression, the only unknown is the nondimensional variable that expresses the values for time and displacement. The remaining temperatures and physical properties are known. However, the equation can not be solved analytically, and a numerical solution is necessary.

A simple Newton method is used to find  $\delta$  by iteration. The iterations run through different values of  $\theta$ , which correspond to different values of  $T_s$  and  $T_b$ , the initial temperatures at the end of the solid and liquid regions, respectively.

The temperature profiles and their corresponding position are presented in the following figures. For each figure, the temperature at the infinite end of the solid region,  $T_s$  is kept constant, while the temperature  $T_l$  in the liquid is varied to study the motion of the solidification interface. As mentioned above, a motion into the solid region is represented by a negative displacement and a motion into the liquid is represented by a positive displacement in  $x$ .

The first three figures show continuous solidification of the liquid. The fourth figure show motion of the boundary line into the solid region, indicating further melting. This is desirable in small depths in order to provide a strong weldline.

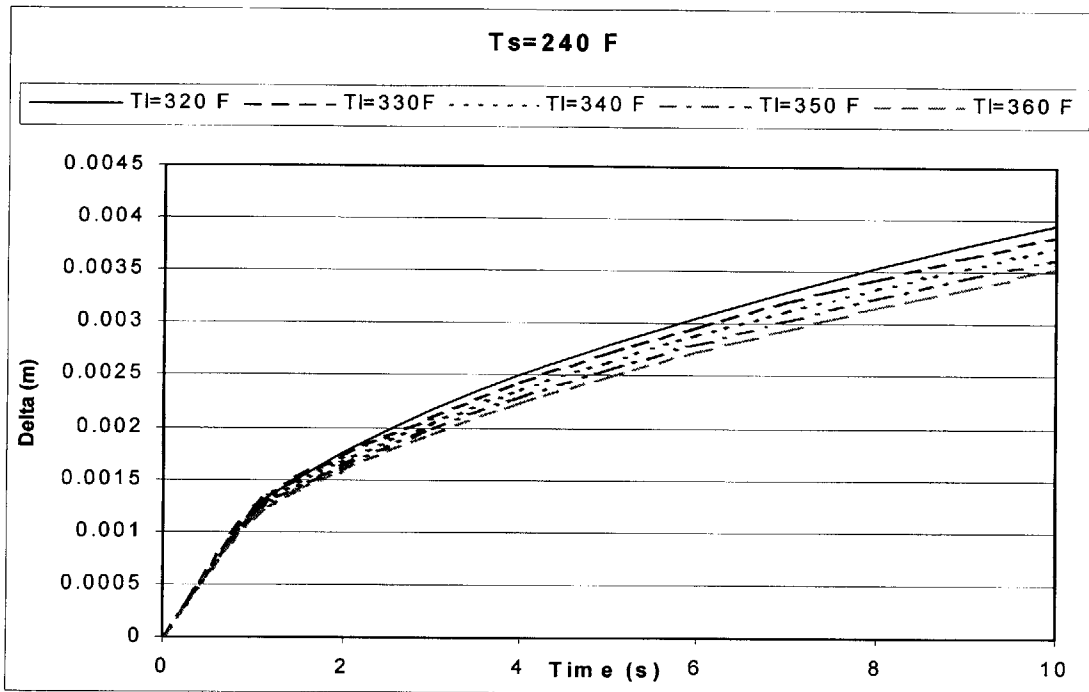


**Figure 3.5** Motion of solidification front for different  $T_m/T_l$  combinations ( $T_s=240$ )

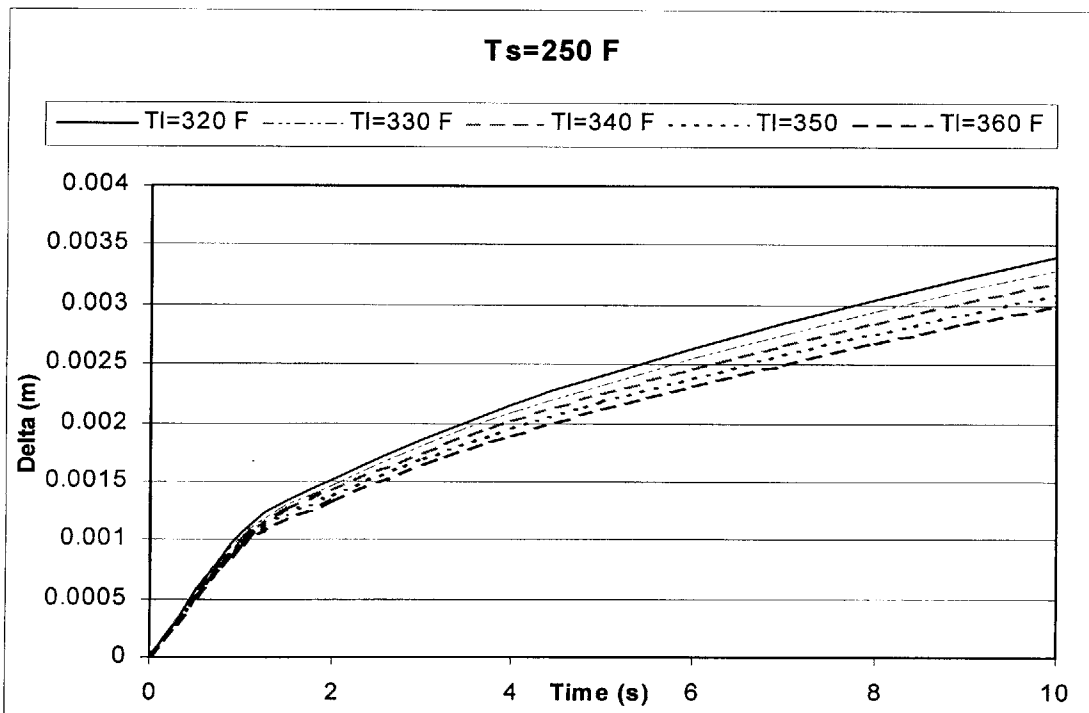


**Figure 3.6** Motion of solidification front for different  $T_m/T_l$  combinations ( $T_s=250$ )

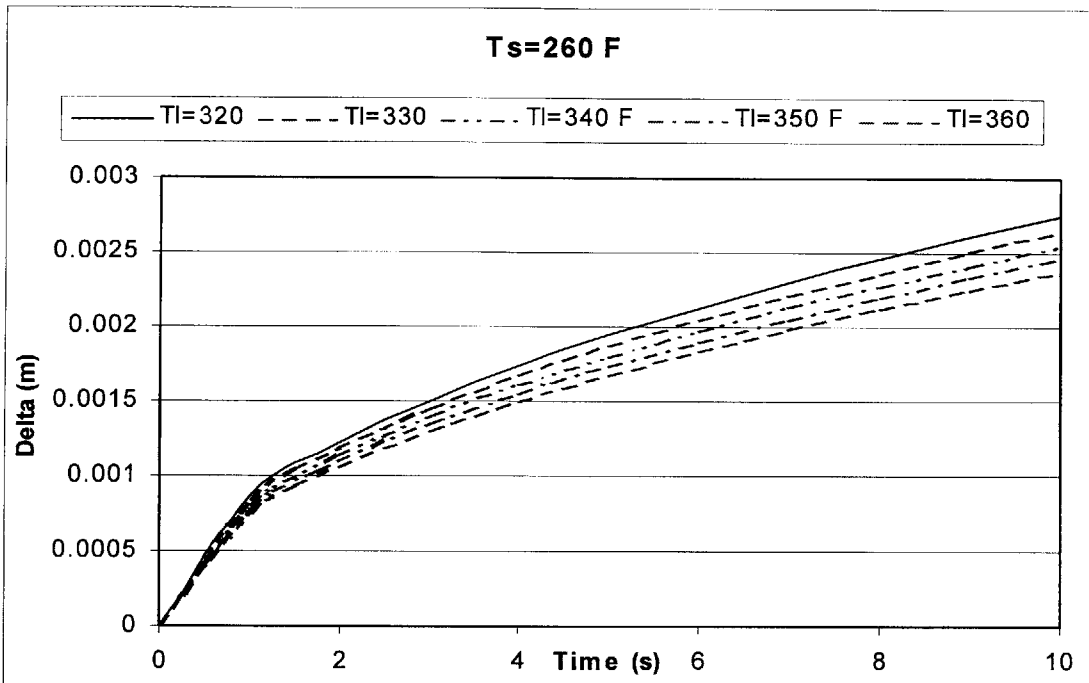


**Figure 3.7** Motion of solidification front for different  $T_m/T_l$  combinations ( $T_s=260$ )

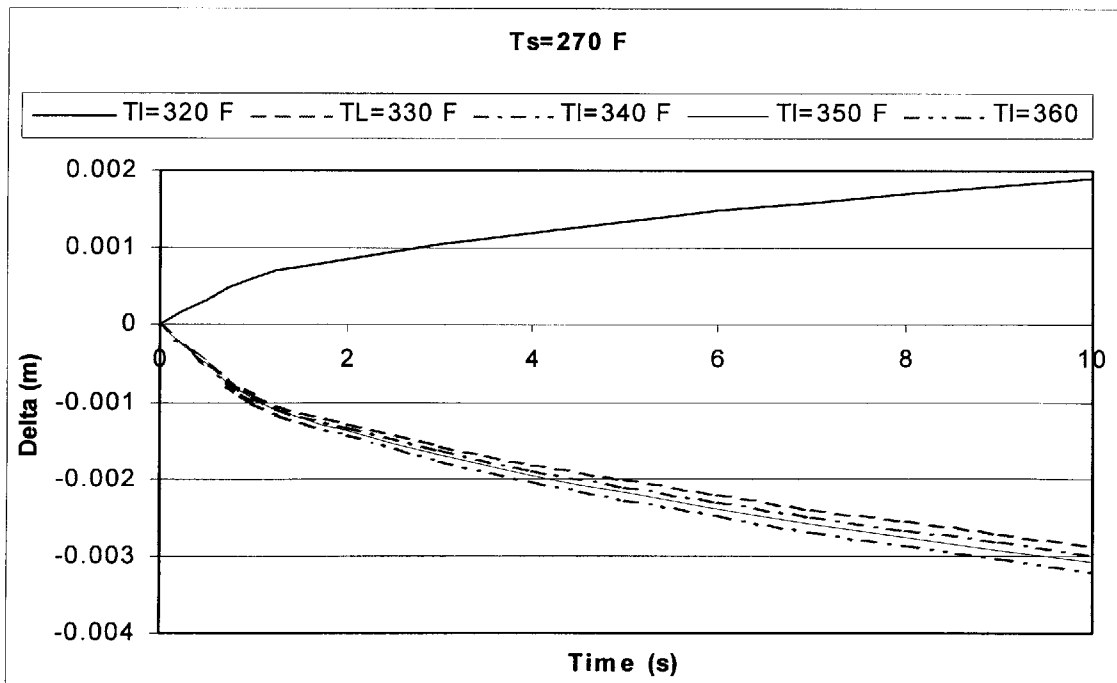


**Figure 3.8** Motion of solidification front for different  $T_m/T_l$  combinations ( $T_s=270$ )

These figures show that there are certain combinations of temperatures for which the solidification line will continue receding.

### 3.4 Solidification front velocity

The relation between time and distance also allows the determination of the front velocity. This velocity can then be compared to the molecular growth velocity determined in the previous chapter, which depends on the interlamellar spacing of the alloy.

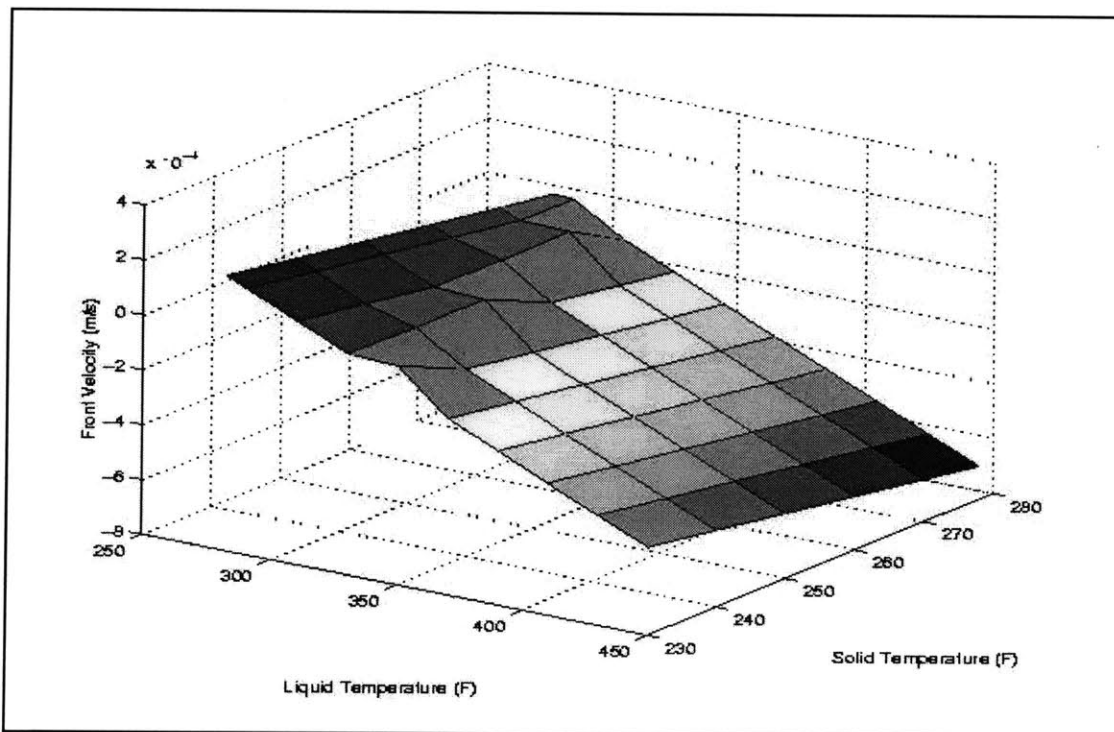


**Figure 3.9** Front velocity for given solid and liquid temperatures

### 3.5 Flow over the stock piece

For the case when the injected liquid flows over the stock piece, this piece needs to be accounted for. Conduction through this body is also modeled in this case to determine which temperatures would be high enough to melt the solid alloy behind the block (which

is undesirable). This can be determined through heat transfer balance between the liquid and the stock, and between the stock and the solid alloy.

If the same heat transfer occurred through all three regions, there would be no phase change in the alloy.

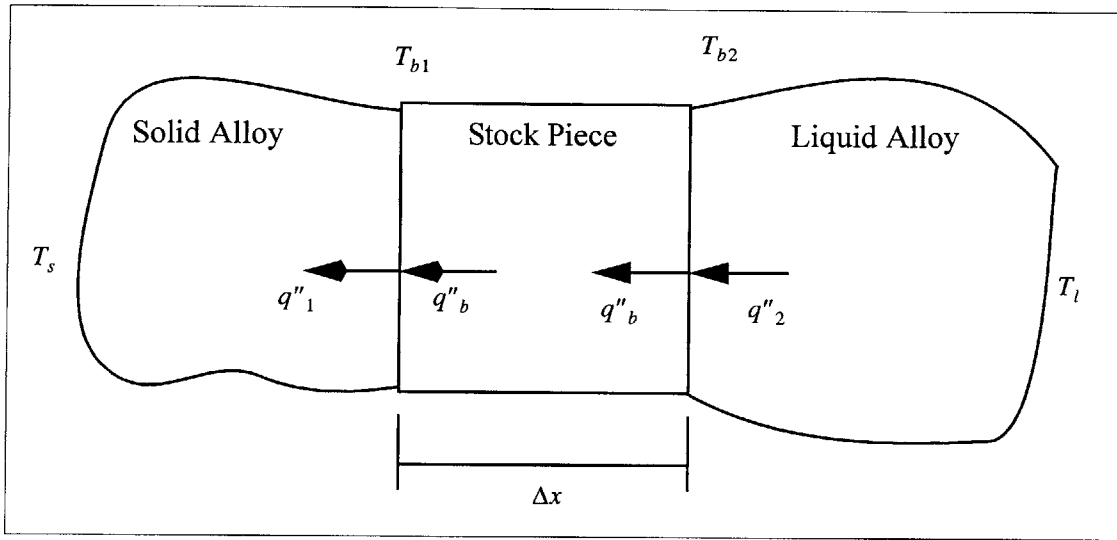


**Figure 3.10** Heat transfer model including an embedded stock piece

The heat flux or heat transfer in each region is given by

$$q''_b = -k_s \frac{(T_{b2} - T_{b1})}{\Delta x}$$

$$q''_1 = \frac{k_1(T_{b1} - T_s)}{\sqrt{\pi\alpha_1 t}}$$

$$q''_2 = \frac{k_2(T_l - T_{b2})}{\sqrt{\pi\alpha_1 t}}$$

At equilibrium, the heat transfer is the same across all regions:  $q''_2 = q''_b = q''_1$

Melting of the solid alloy would start if the heat transfer from the stock block was greater than that into the solid alloy:  $q''_b > q''_1$ . Since the temperatures at the block are unknown, this heat transfer is obtained by relation to the heat transfer from the liquid alloy. It is assumed that they are equal  $q''_b = q''_2$ , which is the limiting case (if the block



heat transfer was larger, the liquid would just solidify and there would be no risk of melting the alloy behind the stock). This equality determines the temperature  $T_{b2}$ :

$$T_{b2} = \frac{\Delta x k_2 T_l + \sqrt{\pi \alpha_2 t} k_s T_{b1}}{\Delta x k_2 + \sqrt{\pi \alpha_2 t} k_s}$$

Introducing this value into the above inequality, it is possible to obtain an expression of  $T_l$ ,  $T_s$  and  $T_{b1}$  for which there is melting of the solid alloy:

$$T_l > \left( 1 + \frac{k_1 \Delta x}{k_s \sqrt{\pi \alpha_1 t}} + \frac{k_1}{k_2} \sqrt{\frac{\alpha_2}{\alpha_1}} \right) T_{b1} - \left( \frac{k_1 \Delta x}{k_s \sqrt{\pi \alpha_1 t}} + \frac{k_1}{k_2} \sqrt{\frac{\alpha_2}{\alpha_1}} \right) T_x.$$

The material properties are known, the stock depth and time can be measured or estimated. The numerical values resulting from this expression correspond to the specific geometry ( $\Delta x$ ) and time of the remolding case under study ( $t$ ,  $T_b$ ). It is thus desired to avoid a combination that will satisfy this inequality.

## Chapter 4

### Experimental Determination of Weldline Strength

Weldline strength carries an important weight in the effectiveness of RFPE during the remolding step. Due to the nature of the process, the parts undergoing remolding are different every time and thus so are the volumes of liquid and solid alloy. To determine a case specific set of temperatures that result in a strong weldline would be a laborious task. Determination of part-specific settings would also contradict the “universal” nature of RFPE. It is thus necessary to find a universal method to measure the strength of the weldline in a remolded part. This quantification would then allow a comparison of the different temperatures used in the making of a part and the determination of the optimal set of temperatures that produce the strongest weldline.

#### 4.1 Optimal weldline strength measurement

An added complexity to the measurement of weldline strength is the variability in size and location of the embedded stock piece. A complex machined piece can be an obstacle to the flow of the injected liquid alloy. It may cause increased turbulence in the flow and induce the presence of air bubbles or pitting. However, once it solidifies, the encapsulant is the main element to hold the remolded block. The relevant strength is then the one related to the adhesion of the liquid alloy to the solid alloy. In a comparison of the encapsulation of different pieces, or during different remolding steps for a same piece, it is thus sufficient to compare the weldline on the alloy rather than considering the adhesion to the stock. This does not neglect the presence of the stock, as the alloy adhesion to its surface is as good as in the first shot.

Testing and quantifying this strength under machining conditions would provide a realistic estimate of its capabilities. However, this would require intensive testing, machining and the use of larger amounts of material. Another effective way of quantifying the weldline strength is performing tensile tests on remolded samples. The ultimate tensile strength of the samples can be compared to each other and to a reference sample made of a single shot of the alloy (without remolding there is no weldline present).

This test can be easily implemented by designing a mold with an adequate shape for tensile tests and preparing the samples with a weldline at the horizontal symmetry plane.

#### **4.2 Sample preparation and test**

The samples were to be tested in an INSTRON machine with conventional grips, so they were prepared to satisfy the ASTM standards.

The mold used to prepare the samples was made of Mica 1100. The machinability of this ceramic is similar to that of stainless steel. Its extremely low coefficient of thermal conductivity prevents it from reaching high temperatures in its exterior. This allows an easy manipulation of such a small mold.

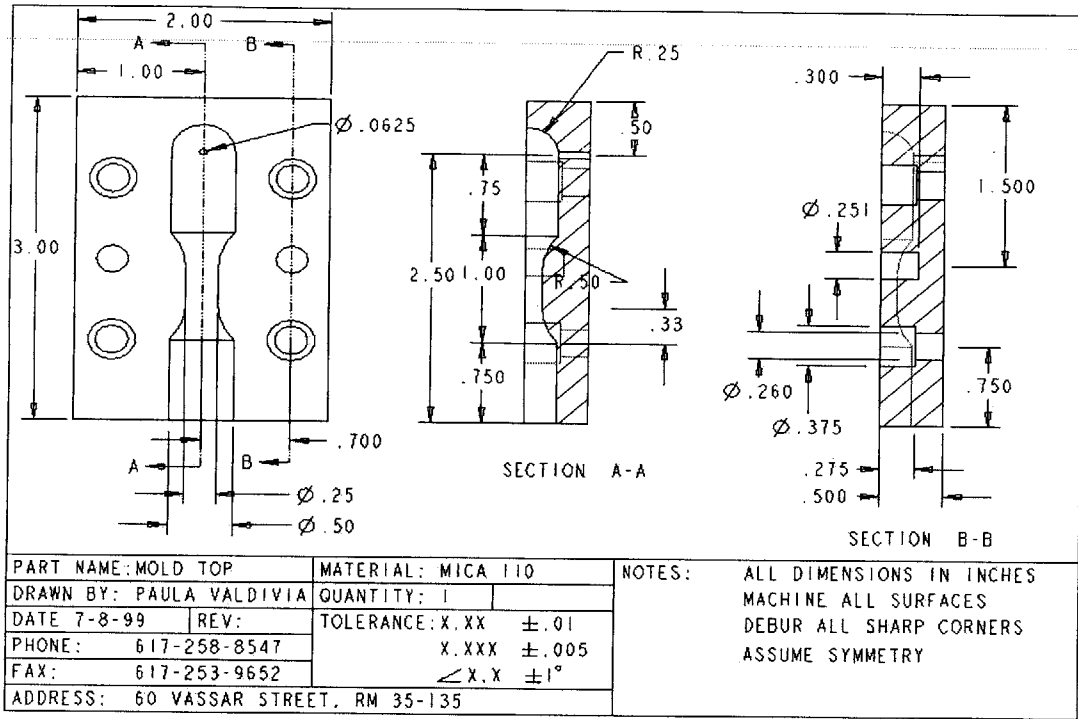


Figure 4.1 Top half of mold

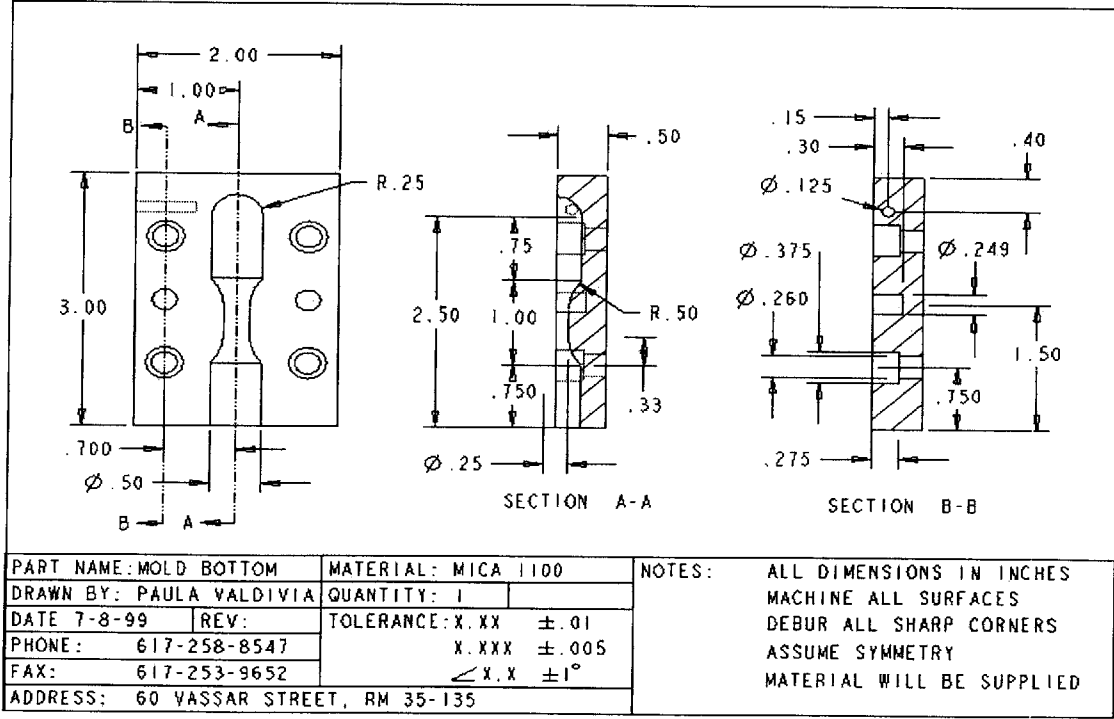
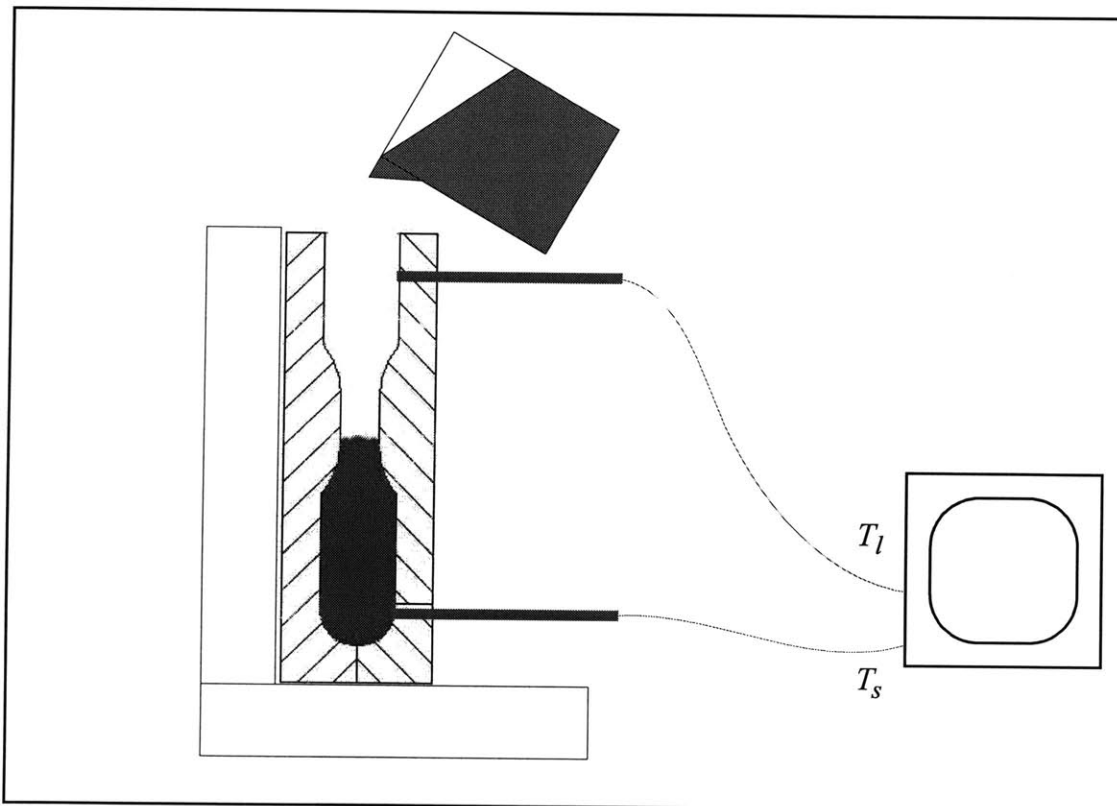


Figure 4.2 Bottom half of mold

Since the sample was small and only the weldline was of interest, the mold was not introduced into the RFPE system for alloy injection. The alloy was hand poured into the mold. The bottom halves were produced first, removed from the mold, sawed at the half plane and reinserted in the mold. Once this step was ready, the liquid alloy was poured again on the solid half and both temperatures were recorded. The procedure is illustrated below:



**Figure 4.3** Pouring of liquid alloy on a previously poured solid half-piece.

Several of the solid bottom halves were pre-heated, their temperatures ranged between ambient and slightly below melting, 279 F. The liquid temperatures varied from slightly above melting temperature up to around 350 F. The temperature combinations of the samples that were prepared are presented below.

ID code	4/11/1	4/4/05	4/4/07	4/13/5	4/14/3	4/13/8	4/14/2	4/14/4	4/14/1	4/4/6
Number	1	2	3	4	5	6	7	8	9	10
Ts (F)	81	70	74	242	233	277	261	98	223	270
Tl (F)	320	287	288	377	359	391	390	308	341	294
$\Delta T$	239	217	214	135	126	114	129	210	118	24
Time to failure (s)	13	12	42	85	134	140	184	181	254	341

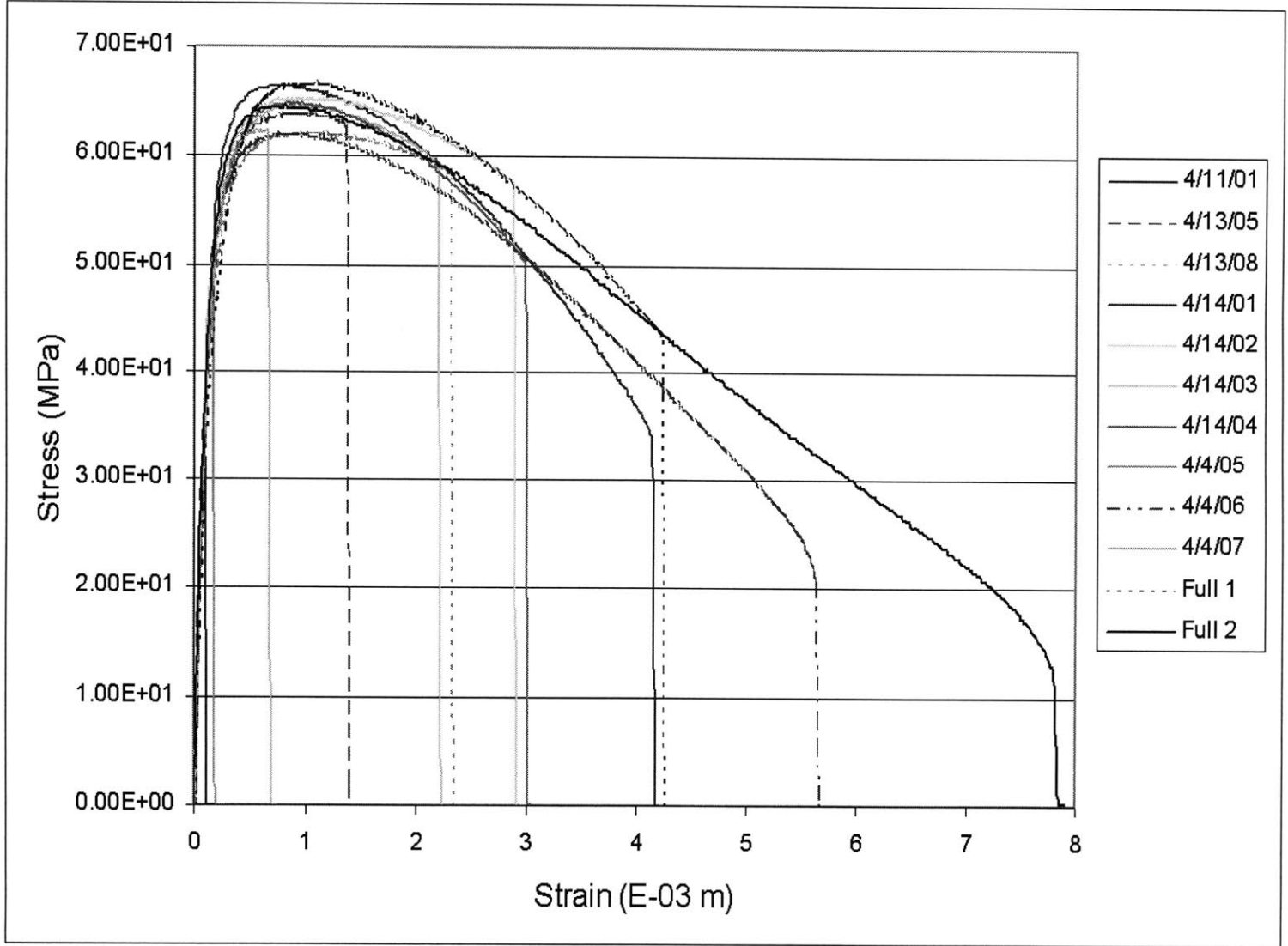
**Table 4.1 Combination of liquid and solid temperatures for each prepared sample**

### 4.3 Tensile test

The testing was conducted in an Instron machine. Simple initial gripping of each sample subjected it to a compression force of about 0.75 kN. This is due to the softness of the material. Besides testing ten samples prepared with a weldline, two full pieces with no weldline were also tested for comparison purposes. As expected, these two lasted longer than all the other samples before failure.

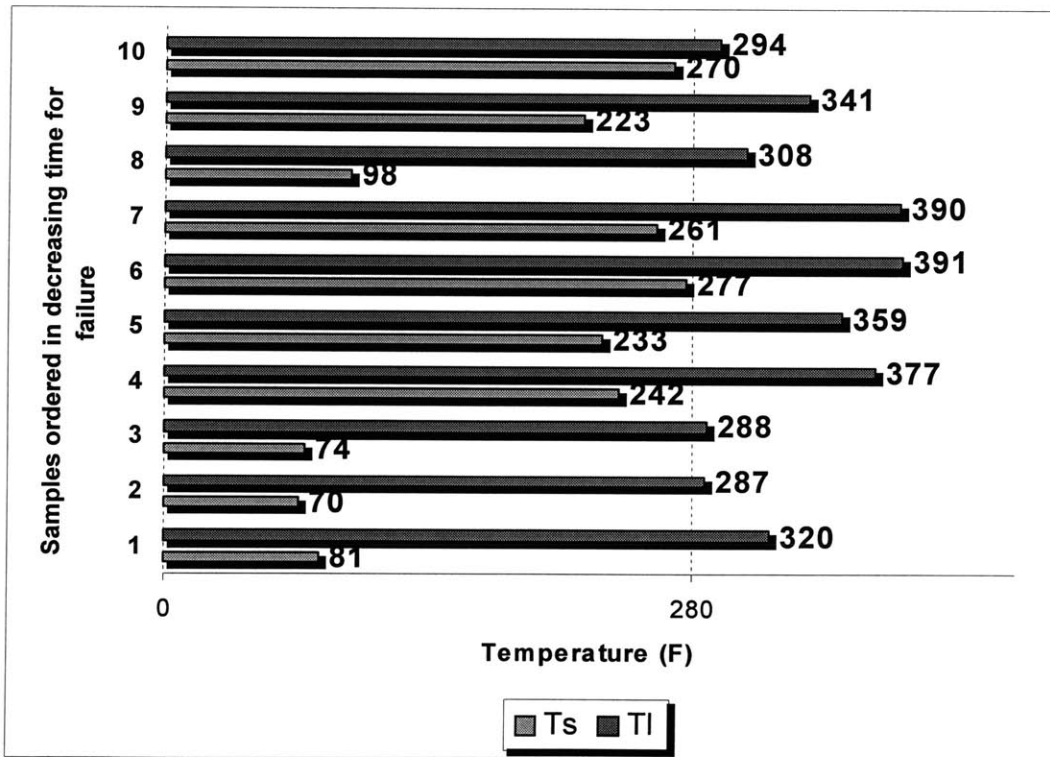
A stress-strain plot including all specimens is presented in Figure 4.4.

Figure 4.4 Comparative stress-strain plot of tested samples.



#### 4.4 Temperature relation

The testing machine increases the load in one-second steps, so the stress and strain values at which each specimen failed also show the relative time at which failure occurred. As expected, the two specimens prepared in a single pour last longer than the rest of the samples (with the exception of one sample). All the samples initially undergo elastic deformation and then considerable plastic deformation. They all fail at different times, which is indicative of the different strain hardening and ductile characteristics of their weldlines. In order to determine which temperatures allow the preparation of a stronger weldline sample, the temperature combinations are presented in the next figure. They are arranged by relative order taken for failure (the smaller number, 1, failed first).



**Figure 4.5** Representation of the order in which samples failed and temperatures at which they were prepared.



The figures do not represent the two samples without weldline, for which temperatures were not recorded. An interesting point of comparison is the difference  $\Delta T$  between  $T_s$  and  $T_l$  in each sample.

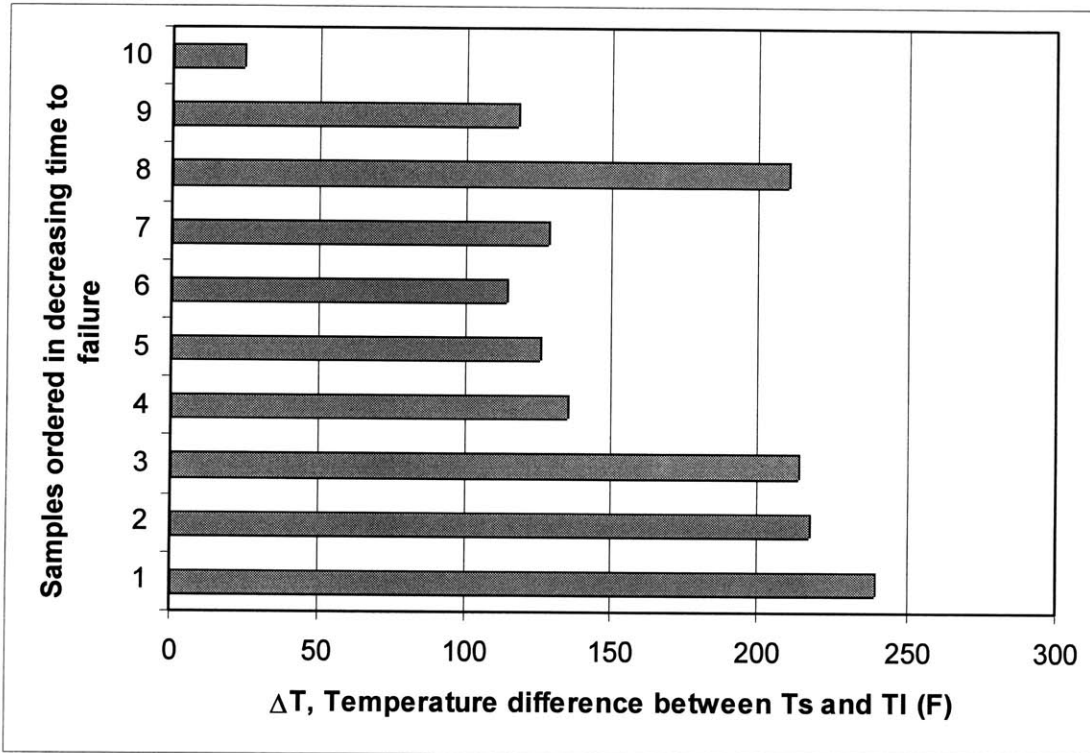


**Figure 4.6** Representation of the order in which samples failed and  $\Delta T$ , the difference between temperatures at which they were prepared

This figure shows that in general, samples with larger  $\Delta T$  failed sooner than those with a smaller temperature difference.

Samples 9, 8 and 7 are somewhat of an exception as they have values of  $\Delta T$  higher than those of the samples that broke later. In the case of samples 9 and 7,  $\Delta T$  is in average only slightly higher than  $\Delta T$  in sample 5 and this can be considered a slight measurement error. However, in the case of sample 8,  $\Delta T$  is considerably larger than in the samples that broke much sooner. In fact, the value of  $\Delta T$  in sample 8 is as high as that of samples 3 and

2, which broke very fast. It is important to note that also, in the case of sample 8, the value of  $T_s$  is in the vicinity of the values of  $T_s$  for samples 1, 2 and 3, which is very close to ambient temperature.

Sample 3 was prepared at temperature conditions similar to those of samples 1 and 2. However, it failed sooner. Sample 3 did not fail at the weldline, but slightly above, which may be indicative of the presence of a crack (whose's growth induced failure).

#### **4.5 Observation of the cross sectional structure**

Another observation to be made is the cross-section of the fractured specimens. The cross section of the samples with fastest failure shows a central granular structure and a lighter outer ring. This ring is the original solid surface present before the liquid was poured onto the solid half. It is thus indicative of lack of remolding in the outer edges of the sample. The samples which showed the strongest weldlines have a darker granular section and, in some cases, a crystal structure. This can be related to the solidification process as described in Chapter 2.

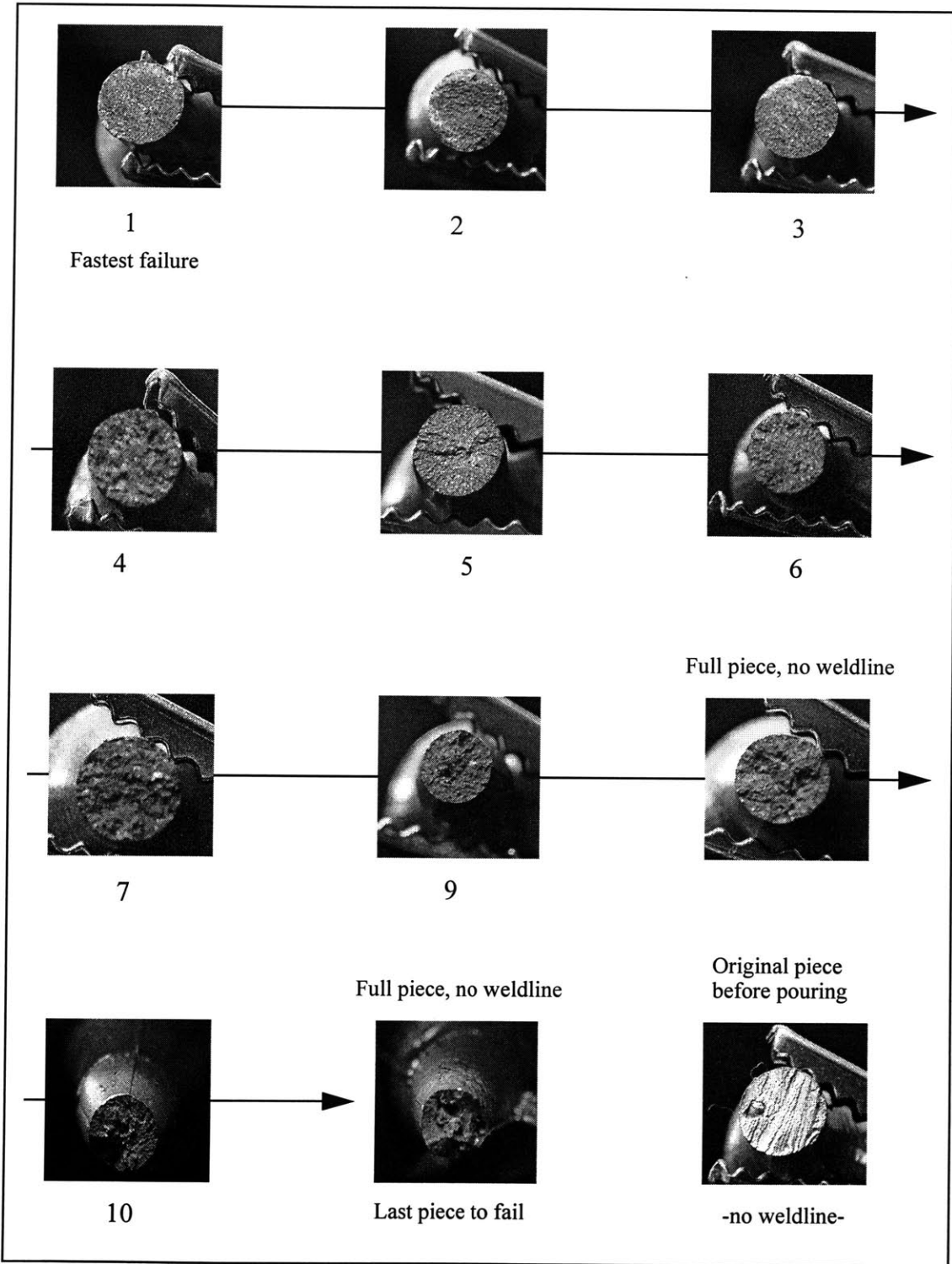


**Figure 4.7** Cross section of tensile test samples: from fastest failure to slowest.

## Chapter 5

### Interpretation of Results and their Application to Remolding in RFPE

The tensile tests showed that the weldline strength varies along with the alloy temperatures and temperature differences at which the sample is prepared. It was also possible to observe the microstructure of solidification created in such weldlines and their relation to the strength. It is now possible to relate the solid and liquid temperatures to the initial phase change and to relate the microstructure to the weldline strength. With such relations, it will become easy to determine the adequate injection parameters for a successful remolding step.

#### 5.1 Relation between temperatures and weldline strength

Figure X shows the relation between time for fracture and  $\Delta T$ , temperature difference between solid and liquid temperatures. Seven of the ten samples agree in showing that a larger values of  $\Delta T$  correspond to a fast failure and thus to a weaker weldline. Similarly, smaller  $\Delta T$  correspond to a stronger weldline, which takes longer to fail in the tensile test. Sample 8 presents an exception to this observation. It has a very high  $\Delta T$ , yet it lasts longer before failure. Despite having similar temperature difference to samples 1, 2 and 3, sample 8 has a much lower .

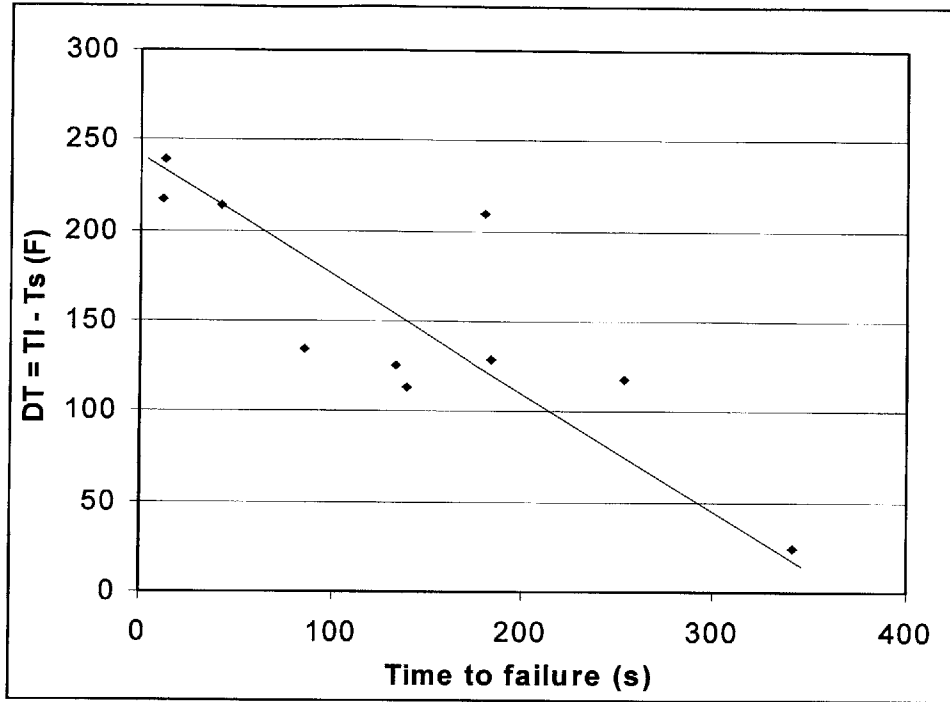


**Figure 5.1** Time to failure vs.  $\Delta T$

Based on the same hypothesis, sample 7 should have failed earlier than sample 6. However, sample 6 did not fail at the weldline. Inspection of the broken sample shows that it failed due to crack growth, and thus its weldline is still stronger than that of sample 7, in consistency with the hypothesis.

These observations make the  $\Delta T$ -weldline strength relation is a good guideline. However, it does not claim to be the most accurate method by itself. Several other considerations must be kept. For instance, samples with similar  $\Delta T$  will have different weldline strength if the values for  $T_s$  and  $T_l$  are of one is considerable lower than the other (for instance a sample with  $T_s$  at ambient temperature and  $T_l$  just above  $T_m$ , compared to a sample where  $T_s$  and  $T_l$  are both much higher).

## 5.2 Microstructure, growth rate and weldline strength

The cross-sections of the broken samples vary in structure. The samples that broke sooner have a fine grain structure, resembling an equiaxed zone. Such a high number of nuclei should indicate a stronger weldline, however the weakness is due to a lack of complete welding on some of the edges.

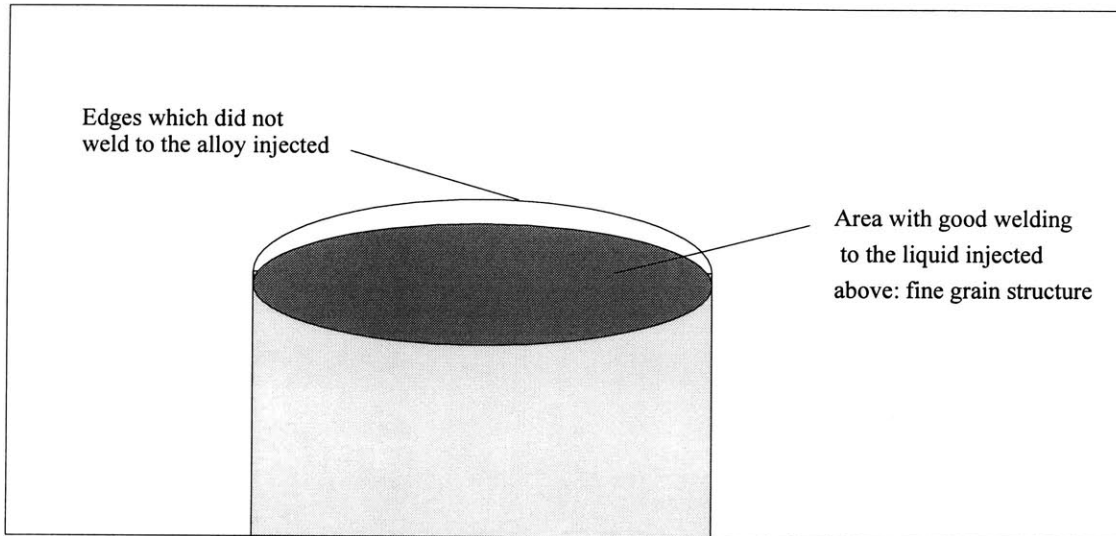


**Figure 5.2** Cross-section of a sample with fast fracture

These edges behave as cracks in the body during the tensile tests and are responsible for the part's failure. Those samples had low values of  $T_s$  and  $T_l$  and a large  $\Delta T$ .

Samples 4 through 8 show a coarser structure, which seems to be the columnar zone. Relative to the previous, finer structure samples, these should be weaker. However, these show bonding through the entire surface, lacking the presence of cracks to make it weaker. On the other hand, the pieces which proved to be stronger also had a fine grain structure, equivalent to an equiaxed zone. These samples did not have cracks on the same plane as the weldline.

Therefore the relation between microstructure and weldline strength grants higher strength to finer grains, provided that there are no other cracks or imperfections in the sample. In order to benefit from this relation, it is necessary to have control over the process that results in such microstructure. It would thus be useful to implement a grain refining method. Some of this methods are industrially used and they fall into Thermal, Mechanical and Chemical refinement groups. These methods promote a fine equiaxed structure mainly by

- a) solidifying alloys with strong solute partitioning and promoting the formation of necked-shaped crystals by preventing growth along the mold wall,
- b) using a low pouring temperature to prevent remelting of crystals released into the liquid and sometimes
- c) enhancing crystal separation by fluid motion in the liquid.

Some of these methods are harder to implement than others, especially in the RFPE setup. Some of the Mechanical methods are ultrasonic irradiation of the fluid, control over feeding geometries and surfaces, mold vibration and liquid stirring. The last two are evidently difficult to implement in a clamped mold. Among the Thermal refinement methods, heat flow control is the most applicable to our setting.

Selecting and implementing one of this refinement methods would ensure a finer grain and stronger weldline in remolded samples.

### **5.3 Conclusion**

Facing the shortcomings of remolding during RFPE brought up the necessity for optimization of that step. Some issues were simpler to address than others. CTE mismatching was solved with an appropriate material selection. On the other hand, the study and optimization of the remolding weldline strength presented itself as a more complex task. The

phenomenons that occur during remolding involve fluid flow, heat and mass transfer and microstructural phase change. A complete study of all these situations was avoided, as RFPE is intended as a universal process where each sample is expected to present a different geometry or material. The heat transfer and microstructural solidification were visited in order to determine their relation to weldline strength and thus determine the best temperature settings during remolding. As a result, we provide guidelines for temperature selection and recommend the implementation of additional refining methods to improve the grain structure of solidification.





Room 14-0551  
77 Massachusetts Avenue  
Cambridge, MA 02139  
Ph: 617.253.2800  
Email: docs@mit.edu  
<http://libraries.mit.edu/docs>

## **DISCLAIMER**

**MISSING PAGE(S)**

56

## References

- [1] Arpaci, V. S. *Conduction Heat Transfer, Abridged Edition*. Ginn Press, Nedham Heights, MA, 1991.
- [2] Alloy Digest. *Data on World Wide Metals and Alloys*. Engineering Alloys Digest, Upper Montclair, NJ, 1980.
- [3] Boyes, William E. *Handbook of jig and fixture design*. Society of Manufacturing Engineers, Dearborn, MI, 1989
- [4] Caram, R, de Castro, W. B., Oliveira, M. F. and Kiminami, C. S. *Microstructure of Undercooled Sn-Se and Sn-Bi alloys*. Proceedings of 4th Decennial International Conference on Solidification Processing, Sheffield, England, V.1, p.485-487, 1997.
- [5] Carslaw, H. S. & Jaeger, J. C. *Conduction of Heat in Solids*. Oxford University Press, 1959.
- [6] Elliot, Roy. *Eutectic Solidification Processing*. Butterworths, 1983
- [7] Esikova, M. B., Iliev, O. P. and Vabishchevich, P. N. *Numerical Investigation of Convection/Diffusion Phase Change of a Metal with Temperature-Dependent Viscosity*. Communications in Applied Numerical Methods, Vol. 8, 857-868, 1992.
- [8] Grigull, U. & Sandner, H. *Heat Conduction*, Springer-Verlag, 1984.
- [9] Hasegawa, M. and Watabe, M. *Theory of Thermodynamic Properties of Liquid Metals*. Journal of the Physical Society of Japan, Vol. 36, No. 6, June, 1974.
- [10] Hill, James M., *One-dimensional Stefan Problems: an Introduction*. Longman Scientific & Technical, 1987.
- [11] Kumari, M. & Dass, N. *Temperature Dependence of Density and Thermal Expansion in Some Liquid Metals*. Journal of Non-Crystalline Solids 156-158, p. 417-420, 1993.
- [12] Lee, Elmer C. *Development of an Encapsulation Process for use in a Universal Automated Fixturing System*. Master of Science Thesis, Massachusetts Institute of Technology, Cambridge, MA, 1999.
- [13] Porter, David A., Easterling, Kenneth E. *Phase Transformations in Metals and Alloys*. Van Nostrand Reinhold Co., New York, NY, 1981.

- [14] Ramachandran, N., Gupta, J. P. and Jaluria, Y. *Thermal and Fluid Flow Effects During Solidification in a Rectangular Enclosure*. International Journal of Heat and Mass Transfer, Vol. 25, p. 187-194, 1982.
- [15] Stellar Industries. *Total Thermal Management*. Leominster, MA
- [16] Vabishchevich, P., Iliev, O. *Numerical Investigation of Heat and Mass Transfer During the Crystallization of Metal in a Mould*. Communications in Applied Numerical Methods, Vol. 5, 515-526, 1989.
- [17] Vol, A. E. *Handbook of binary metallic systems: structure and properties*. Israel Program for Scientific Translations, Jerusalem, 1966-1967.
- [18] Voller, V. R., Markatos, N. C. and Cross, M. *Solidification in Convection-Diffusion*. Centre for Numerical Modelling and Process Analysis, Thames Polytechnic, London SE18 6PF.
- [19] Wilson, D. G., Solomon, A. D. and Alexiades, V. *A Model of Binary Alloy Solidification*. International Journal for Numerical Methods in Engineering, Vol. 20, p.1067-1084, 1984.
- [20] Wilson, Frank W., American Society of Tool and Manufacturing Engineers. *Handbook of fixture design; a practical reference book of workholding principles and designs for all classes of machining, assembly, and inspection*. McGraw-Hill, New York, 1962.